Deep-inelastic and quasielastic electron scattering from $A = 3$ nuclei

A. J. Tropiano,[1] J. J. Ethier,[2] W. Melnitchouk,[3] and N. Sato[3,4,5]
[1]*The Ohio State University, Columbus, Ohio 43210, USA*
[2]*Department of Physics and Astronomy, Vrije Universiteit Amsterdam, 1081 HV Amsterdam and Nikhef Theory Group, Science Park 105, 1098 XG Amsterdam, The Netherlands*
[3]*Jefferson Lab, Newport News, Virginia 23606, USA*
[4]*University of Connecticut, Storrs, Connecticut 06269, USA*
[5]*Old Dominion University, Norfolk, Virginia 23529, USA*

(Received 19 November 2018; published 1 March 2019)

We perform a combined analysis of inclusive electron scattering data from $A = 3$ nuclei in the deep-inelastic and quasielastic scattering regions, using Monte Carlo analysis methods and the nuclear weak binding approximation to establish the range over which the data can be described within the same theoretical framework. Comparison with quasielastic ^{3}He cross sections from SLAC and Jefferson Lab suggests that most features of the $x \gtrsim 1$ data can be reasonably well described in the impulse approximation with finite-Q^2 nuclear smearing functions for momentum transfers $Q^2 \gtrsim 1$ GeV^2. For the DIS region, we analyze the recent ^{3}He to deuterium cross-section ratio from the Jefferson Lab E03-103 experiment to explore the possible isospin dependence of the nuclear effects. We discuss the implications of this for the MARATHON experiment at Jefferson Lab and outline how a Bayesian analysis of ^{3}He, ^{3}H, and deuterium data can robustly determine the free neutron structure function.

DOI: 10.1103/PhysRevC.99.035201

I. INTRODUCTION

With the completion of the 12 GeV energy upgrade of Jefferson Lab, a new chapter in the exploration of the quark structure of the nucleon and nuclei has begun. One of the main drivers of the new facility is the determination of the spatial, momentum, and spin distributions of the nucleon's valence quarks. Of particular interest are configurations in which a single quark carries a large fraction, x, of the momentum of the nucleon, which can reveal details of the underlying quark-gluon dynamics [1].

It is surprising that, almost four decades after the first experimental deep-inelastic scattering (DIS) programs were initiated, such fundamental quantities as the momentum fraction carried by d quarks in the proton are still poorly known at large x [2–4]. While this is partly due to the steeply falling inclusive DIS rates as $x \to 1$, the additional complication has been the absence of free neutron targets, which has significantly limited the extraction of u and d flavor information from hydrogen and deuterium data due to nuclear effects in the latter [5]. Indeed, uncertainties from the short-range part of the nucleon-nucleon interaction give rise to differences in the extracted d/u parton distribution function (PDF) ratio that are typically of the same order as the variation between predictions from different dynamical models [6–8].

Recent progress on the experimental front has come with the measurement of the nearly free neutron structure function in the "BONuS" experiment at Jefferson Lab [9,10], using spectator tagging in semi-inclusive DIS from the deuteron, which has improved the precision of the d/u ratio in the intermediate- to high-x region. More dramatically, data on charged lepton and W-boson asymmetries in $p\bar{p}$ collisions from the CDF and D0 Collaborations at Fermilab [11–14] have provided more stringent constraints on the d/u behavior up to $x \sim 0.7$. In particular, the recent CJ15 global QCD analysis [15] suggested that the nucleon off-shell effects in the deuteron are relatively small, at least in the isoscalar channel.

However, while the new data have led to a reduction in the extracted PDF uncertainties at large x, there is still considerable uncertainty in the extrapolation from the highest x values at which there are data to the $x = 1$ limit. For instance, depending on the functional form chosen for the u and d PDFs, one can get rather different extrapolated d/u ratios in the $x = 1$ limit [15,16]. The experimental program at Jefferson Lab at 12 GeV aims to bridge this gap by using several novel techniques to isolate the d/u ratio up to $x \sim 0.85$ in the DIS region. The spectator tagging method will be used again to extend the BONuS experiment to 12 GeV [17], isolating nearly free neutrons in the deuteron by detecting a low-momentum, backward-angle proton in DIS off deuterium. Further ahead, the SoLID Collaboration aims to measure parity-violating DIS from the proton, with the γ-Z interference structure function providing a different combination of the u and d PDFs compared with electromagnetic scattering [18,19].

In this paper, we consider the alternative method proposed to extract the d/u ratio, using the measurement of DIS cross sections from ^{3}He and ^{3}H nuclei with the MARATHON experiment at Jefferson Lab [20], which completed data taking in 2018. It was shown in Refs. [21–24] that, under reasonable assumptions about the isospin dependence of nucleon off-

shell effects, the ratio of ^{3}He to ^{3}H structure functions could directly constrain the neutron to proton ratio, F_2^n/F_2^p, with nuclear effects largely canceling between the mirror nuclei. From knowledge of the free neutron to proton ratio, one can then directly extract d/u in the valence-quark-dominated region, $x \gtrsim 0.4$.

Since the earlier calculations, progress on the theoretical front has been made in computing structure functions of light nuclei within the framework of the weak binding approximation (WBA) [25–27], including finite-energy corrections and nucleon off-shell contributions. In the case of the DIS from the deuteron, the latter have been estimated within nuclear models [6,7] and fitted in phenomenological analyses [15,16,25] for a given set of deuteron wave functions. Information on the off-shell effects in $A = 3$ nuclei, on the other hand, has been more difficult to obtain, partly because of the dearth of data on unpolarized ^{3}He structure functions (and the complete absence for ^{3}H). This had left open the possibility of potentially large isovector off-shell effects [24], which would contribute to ^{3}He/^{3}H structure functions, but not be seen in DIS from deuterium. (For early work that considered quark-gluon effects in scattering from $A = 3$ nuclei, see Refs. [28–32].)

In the present work, we revisit the question of the isospin dependence of off-shell effects in the light of more recent data from the Jefferson Lab E03-103 experiment [33], which measured ratios of structure functions of light nuclei to those of deuterium. In particular, the experiment obtained the first high-precision determination of the ^{3}He to deuterium cross-section ratio for $x \sim 0.3$–0.6 in DIS kinematics. These data have the potential to constrain, when combined with the inclusive deuterium DIS data, the individual off-shell corrections to the proton and neutron structure functions and clarify the impact on the extracted F_2^n/F_2^p ratio. In Ref. [34], for example, the data were used to benchmark the n/p ratio extracted from E03-103 with that obtained from earlier inclusive proton and deuterium data sets, requiring a "renormalization" of the ^{3}He to deuterium cross-section ratio by $+3\%$. Here, we re-examine the E03-103 ^{3}He/deuterium data, in combination with the isoscalar nucleon off-shell corrections obtained from the recent CJ15 global QCD analysis [15], and place upper limits on the magnitude of the isospin dependence of the off-shell corrections.

To further constrain the models of the nuclear effects, we test the efficacy of the ^{3}He smearing functions computed within the WBA framework to simultaneously describe other processes, such as quasielastic (QE) electron scattering from ^{3}He nuclei. We compare with the available QE data from experiments at SLAC [35,36] and Jefferson Lab [37] in the region $x \gtrsim 1$ and at four-momentum transfers $Q^2 \sim 1$ to a few GeV^2, where the nuclear impulse approximation is expected to be valid.

We begin in Sec. II by reviewing the formalism for inclusive lepton scattering from nuclei, and summarizing the results for nuclear structure functions in terms of on-shell and off-shell convolutions of nucleon structure functions and nucleon (light-cone) momentum distribution functions in $A = 3$ nuclei. Here we also illustrate the specific features of the nucleon light cone distributions (which are also referred to as nucleon "smearing functions") as a function of nuclear momentum fraction and Q^2. The versatility of the smearing functions in describing different ^{3}He observables is discussed in Sec. III, where we compare the QE cross sections calculated in the WBA with data on inclusive electron-^{3}He scattering in the QE region, $x \sim 1$, from SLAC [35,36] and Jefferson Lab [37]. After establishing the kinematic regions in x and Q^2 where the data can be accommodated, we estimate the QE cross sections for ^{3}He and ^{3}H at the kinematics of the E12-11-112 experiment at Jefferson Lab [38].

DIS from ^{3}He and ^{3}H nuclei is discussed in Sec. IV. Here we fit the recent 6-GeV Jefferson Lab data [33] on the ^{3}He to deuterium cross-section ratio to extract the isovector component of the nucleon off-shell contributions. We use several different nuclear models and off-shell parametrizations to estimate the theoretical uncertainty in the extracted off-shell corrections and determine the impact on the extraction of the F_2^n/F_2^p ratio. Finally, in Sec. V we summarize our findings and anticipate future developments in experiment and theory which may reveal further insight into both the quark structure of the nucleon and the dynamics of ^{3}He and ^{3}H nuclei.

II. FORMALISM

In this section, we summarize the basic formulas for inclusive electron scattering from nuclei. We present the results for the nuclear structure functions in the framework of the WBA, in which the structure functions of the nucleus are represented as convolutions of nucleon momentum distributions in the nucleus and structure functions of (off-shell) nucleons, up to $\mathcal{O}(\boldsymbol{p}^2/M^2)$ corrections, where $\boldsymbol{p}$ and M are the 3-momentum and mass of the initial state nucleon [25,26,39–41]. (Higher order relativistic effects necessarily lead to a breakdown of the factorization embodied in the convolution representation [42,43].) After providing the complete set of formulas for structure functions for scattering of both transverse and longitudinal photons, we illustrate the smearing functions, for on-shell and off-shell nucleon contributions, for $A = 3$ nuclei.

A. Inclusive nuclear cross section and structure functions

We consider the inclusive scattering of an electron from a nucleus A (later specializing to the case $A =$ ^{3}He and ^{3}H), $eA \to eX$, where X represents the unobserved hadronic state. We denote the four-momenta of the incident and scattered electrons by k_μ and k'_μ, respectively, and the four-momentum of the target by P_μ. In the target rest frame, the inclusive cross section is given by

$$\frac{d^2\sigma}{d\Omega dE'} = \frac{\alpha^2}{Q^4}\frac{E'}{E}\frac{1}{M_A} L_{\mu\nu} W^{\mu\nu}, \tag{1}$$

where α is the fine structure constant, E (E') is the energy of the incident (scattered) electron, and M_A is the mass of the nucleus. The four-momentum of the exchanged virtual photon is $q_\mu = k_\mu - k'_\mu$. The invariant mass squared of the photon can be approximated by neglecting the small electron mass,

$Q^2 \equiv -q^2 \approx 4EE' \sin^2(\theta/2)$, where θ is the angle between the incident and scattered electrons. The leptonic tensor in Eq. (1) is given by

$$L_{\mu\nu} = 2k_\mu k'_\nu + 2k'_\mu k_\nu + q^2 g_{\mu\nu}, \tag{2}$$

and the hadronic tensor is parametrized by the nuclear structure functions F_1^A and F_2^A,

$$W^{\mu\nu}(P,q) = \left(-g^{\mu\nu} + \frac{q^\mu q^\nu}{q^2}\right) F_1^A + \left(P^\mu - \frac{P\cdot q}{q^2} q^\mu\right)\left(P^\nu - \frac{P\cdot q}{q^2} q^\nu\right)\frac{F_2^A}{P\cdot q}. \tag{3}$$

The structure functions are taken to be functions of Q^2 and the Bjorken scaling variable, $x = Q^2/2M\nu$, where $\nu = E - E'$ is the energy transfer. One can then write the inclusive cross section in terms of the nuclear structure functions as

$$\sigma^A \equiv \frac{d^2\sigma}{d\Omega dE'} = \sigma_{\rm Mott}\left[\frac{2}{M_A}\tan^2\frac{\theta}{2} F_1^A(x,Q^2) + \frac{1}{\nu} F_2^A(x,Q^2)\right], \tag{4}$$

where $\sigma_{\rm Mott} = (4\alpha^2 E'^2/Q^4)\cos^2(\theta/2)$ is the Mott cross section for scattering from a point particle. Note that for forward scattering, $\theta = 0^\circ$, the cross section is dominated by the F_2^A structure function, while for backward scattering, $\theta = 180^\circ$, it is given only in terms of F_1^A. For intermediate scattering angles, both the F_1^A and F_2^A structure functions contribute to the cross section.

Alternatively, one can also write the hadronic tensor and cross section in terms of the transverse and longitudinal structure functions, F_T^A and F_L^A, corresponding to the contributions to the scattering from exchanged photons with transverse or longitudinal polarization, respectively,

$$F_T^A(x,Q^2) = 2xF_1^A(x,Q^2), \tag{5a}$$

$$F_L^A(x,Q^2) = \gamma^2 F_2^A(x,Q^2) - F_T^A(x,Q^2), \tag{5b}$$

where the kinematical parameter

$$\gamma^2 \equiv \frac{\boldsymbol{q}^2}{\nu^2} = 1 + \frac{4M^2x^2}{Q^2} \tag{6}$$

accounts for finite-energy effects. The parameter γ is related to the Nachtmann scaling variable [44,45] $\xi = 2x/(1+\gamma)$, which takes into account target mass corrections that arise at finite energy. Note that sometimes in the literature one uses the nuclear scaling variable, $x_A = (M/M_A)x$, which ranges between 0 and 1. In the present analysis, we will use the variable x when comparing structure functions of nuclei and nucleons.

B. Structure functions in the weak binding approximation

Neglecting antinucleon degrees of freedom, in the WBA the nucleus is approximated as a system of weakly bound nucleons with four-momentum $p_\mu \equiv (M+\varepsilon, \boldsymbol{p})$, where the nucleon three-momentum $\boldsymbol{p}$ and off-shell energy energy ε (<0) are both much smaller than the nucleon mass, $|\boldsymbol{p}|, |\varepsilon| \ll M$ [39,40]. Reducing the relativistic Lorentz-Dirac structures in the general decomposition of the off-shell nucleon hadronic tensor [39,42], one can relate the relativistic four-component nucleon field to the corresponding two-component operator, up to order $\mathcal{O}(\boldsymbol{p}^2/M^2)$ [25,26]. The imaginary part of the nucleon propagator can then be written in terms of a nuclear spectral function defined through the correlator of the nonrelativistic fields.

A lengthy but straightforward derivation then allows one to show that the nuclear structure functions can be written in factorized form,

$$xF_1^A(x,Q^2) = \sum_N \int \frac{d^4p}{(2\pi)^4} \mathcal{F}_0^N(\varepsilon,\boldsymbol{p})\left(1 + \frac{\gamma p_z}{M}\right)\left[\mathcal{C}_{11}\frac{x}{y}\widetilde{F}_1^N\left(\frac{x}{y},Q^2,p^2\right) + \mathcal{C}_{12}\widetilde{F}_2^N\left(\frac{x}{y},Q^2,p^2\right)\right], \tag{7a}$$

$$F_2^A(x,Q^2) = \sum_N \int \frac{d^4p}{(2\pi)^4} \mathcal{F}_0^N(\varepsilon,\boldsymbol{p})\left(1 + \frac{\gamma p_z}{M}\right)\mathcal{C}_{22}\widetilde{F}_2^N\left(\frac{x}{y},Q^2,p^2\right), \tag{7b}$$

$$F_L^A(x,Q^2) = \sum_N \int \frac{d^4p}{(2\pi)^4} \mathcal{F}_0^N(\varepsilon,\boldsymbol{p})\left(1 + \frac{\gamma p_z}{M}\right)\left[\mathcal{C}_{LL}\widetilde{F}_L^N\left(\frac{x}{y},Q^2,p^2\right) + \mathcal{C}_{L2}\widetilde{F}_2^N\left(\frac{x}{y},Q^2,p^2\right)\right], \tag{7c}$$

where the sum is over nucleons $N = p, n$, the function $\mathcal{F}_0^N$ is the nonrelativistic nucleon spectral function in the nucleus, and $\widetilde{F}_i^N$ ($i = 1, 2, L$) are the off-shell nucleon structure functions, which depend also on the nucleon virtuality, p^2. The variable

$$y \equiv \frac{M_A}{M}\frac{p\cdot q}{P\cdot q} = \frac{p_0 + \gamma p_z}{M} \tag{8}$$

is the light-cone fraction of the nuclear momentum carried by the interacting nucleon. The coefficients $\mathcal{C}_{ij}$ are given by

$$\mathcal{C}_{11} = 1, \quad \mathcal{C}_{12} = (\gamma^2 - 1)\frac{\boldsymbol{p}_\perp^2}{4y^2M^2}, \quad \mathcal{C}_{22} = \frac{1}{\gamma^2}\left[1 + \frac{(\gamma^2-1)}{2y^2M^2}(2p^2 + 3\boldsymbol{p}_\perp^2)\right], \quad \mathcal{C}_{LL} = 1, \quad \mathcal{C}_{L2} = (\gamma^2-1)\frac{\boldsymbol{p}_\perp^2}{y^2M^2}. \tag{9}$$

Note that while in the $Q^2 \to \infty$ limit all the structure functions are "diagonal," at finite Q^2 the transverse and longitudinal structure functions F_1^A and F_L^A receive contributions from both the nucleon's $\widetilde{F}_1^N$ and $\widetilde{F}_2^N$ (or $\widetilde{F}_L^N$ and $\widetilde{F}_2^N$) structure functions, whereas F_2^A remains diagonal.

The p^2 dependence of the off-shell nucleon structure functions $\widetilde{F}_i^N$ is, in itself, unphysical and must be interpreted in the context of the p^2 dependence of the spectral function $\mathcal{F}_0^N$, such that only the total nuclear structure function is physical. Nevertheless, for a given nuclear wave function model which defines the spectral function, one can extract the off-shell part of the nucleon structure function phenomenologically. For small nucleon virtualities, $|v| \ll 1$, where $v \equiv v(p^2) = (p^2 - M^2)/M^2$, one can expand the off-shell nucleon structure functions in a Taylor series around $p^2 = M^2$,

$$\widetilde{F}_i^N(x, Q^2, p^2) = F_i^N(x, Q^2)\left[1 + v(p^2)\,\delta f_i^N(x, Q^2) + \mathcal{O}(v^2)\right], \quad i = 1, 2, L, \tag{10}$$

where F_i^N are the on-shell nucleon structure functions, and the coefficient of the $O(v)$ term is given by

$$\delta f_i^N(x, Q^2) = \left.\frac{\partial \log \widetilde{F}_i^N(x, Q^2, p^2)}{\partial v(p^2)}\right|_{v=0}. \tag{11}$$

In earlier analyses, the off-shell function δf_i^N was either computed within simple spectator quark models [6,25,40] or extracted from empirical fits to nuclear structure function data [15,16,25] assuming dependence on x only. Furthermore, typically it has been assumed that the same function describes the off-shell modification of both the F_1^N and F_2^N (and F_L^N) structure functions, $\delta f_1^N = \delta f_2^N = \delta f_L^N \equiv \delta f^N$. However, unlike in previous analyses which assumed also the isospin independence of δf^N, here we allow the off-shell corrections for the proton and neutron to differ, $\delta f_i^p \neq \delta f_i^n$.

The Taylor series expansion in Eq. (10) allows the derivation of simple expressions for the nuclear structure functions in terms of on-shell and off-shell convolutions. For the on-shell part, taking the first term in Eq. (10) yields the familiar on-shell convolution approximation to the nuclear structure functions [15,25,46],

$$xF_1^{A\,(\mathrm{on})}(x, Q^2) = \sum_N \int dy \left[f_{11}^N(y, \gamma)\,\frac{x}{y} F_1^N\left(\frac{x}{y}, Q^2\right) + f_{12}^N(y, \gamma)\,F_2^N\left(\frac{x}{y}, Q^2\right)\right], \tag{12a}$$

$$F_2^{A\,(\mathrm{on})}(x, Q^2) = \sum_N \int dy \left[f_{22}^N(y, \gamma)\,F_2^N\left(\frac{x}{y}, Q^2\right)\right], \tag{12b}$$

$$F_L^{A\,(\mathrm{on})}(x, Q^2) = \sum_N \int dy \left[f_{LL}^N(y, \gamma)\,F_L^N\left(\frac{x}{y}, Q^2\right) + f_{L2}^N(y, \gamma)\,F_2^N\left(\frac{x}{y}, Q^2\right)\right], \tag{12c}$$

where the one-dimensional smearing functions are given by

$$f_{ij}^N(y, \gamma) = \int \frac{d^4p}{(2\pi)^4} \mathcal{F}_0^N(\varepsilon, \boldsymbol{p}) \left(1 + \frac{\gamma p_z}{M}\right) C_{ij}\,\delta\left(y - 1 - \frac{\varepsilon + \gamma p_z}{M}\right), \tag{13}$$

and the y integrations in Eqs. (12) range from x to M_A/M. Note that for $\gamma = 1$ the diagonal functions f_{ii}^N $(i = 1, 2, L)$ are normalized to unity, corresponding to the spectral function normalization

$$\int_0^{M_A/M} dy\, f_{ii}^N(y, \gamma = 1) = \int \frac{d^4p}{(2\pi)^4}\, \mathcal{F}_0^N(\varepsilon, \boldsymbol{p}) = 1 \tag{14}$$

for both protons and neutrons, $N = p, n$. Generalizing Eqs. (12) to include the off-shell term in Eq. (10) proportional to v, one can write the first-order off-shell contributions to the nuclear structure functions as [47]

$$xF_1^{A\,(\mathrm{off})}(x, Q^2) = \sum_N \int dy \left[\widetilde{f}_{11}^N(y, \gamma)\,\frac{x}{y} F_1^N\left(\frac{x}{y}, Q^2\right) + \widetilde{f}_{12}^N(y, \gamma)\,F_2^N\left(\frac{x}{y}, Q^2\right)\right] \delta f^N\left(\frac{x}{y}, Q^2\right), \tag{15a}$$

$$F_2^{A\,(\mathrm{off})}(x, Q^2) = \sum_N \int dy \left[\widetilde{f}_{22}^N(y, \gamma)\,F_2^N\left(\frac{x}{y}, Q^2\right)\right] \delta f^N\left(\frac{x}{y}, Q^2\right), \tag{15b}$$

$$xF_L^{A\,(\mathrm{off})}(x, Q^2) = \sum_N \int dy \left[\widetilde{f}_{LL}^N(y, \gamma)\,F_L^N\left(\frac{x}{y}, Q^2\right) + \widetilde{f}_{L2}^N(y, \gamma)\,F_2^N\left(\frac{x}{y}, Q^2\right)\right] \delta f^N\left(\frac{x}{y}, Q^2\right), \tag{15c}$$

where the off-shell smearing functions $\widetilde{f}_{ij}^N$ are defined by including the factor v in the integrand of Eq. (13),

$$\widetilde{f}_{ij}^N(y, \gamma) = \int \frac{d^4p}{(2\pi)^4} \mathcal{F}_0^N(\varepsilon, \boldsymbol{p}) \left(1 + \frac{\gamma p_z}{M}\right) C_{ij}\, v(p^2)\,\delta\left(y - 1 - \frac{\varepsilon + \gamma p_z}{M}\right). \tag{16}$$

The total nuclear structure functions are then given by the sum of the on-shell and off-shell contributions,

$$F_i^A(x,Q^2) = F_i^{A\,(\mathrm{on})}(x,Q^2) + F_i^{A\,(\mathrm{off})}(x,Q^2), \quad i=1,2,L. \tag{17}$$

These results are general and valid for any bound system of A nucleons. With the above normalization for the smearing functions (14), the nuclear structure functions can be written in terms of the proton and neutron contributions as

$$F_i^A(x,Q^2) = ZF_i^{p/A}(x,Q^2) + (A-Z)F_i^{n/A}(x,Q^2), \quad i=1,2,L. \tag{18}$$

In the next section, we specialize to the case of $A=3$ nuclei.

C. Smearing functions for $A=3$ nuclei

In this section, we describe the proton and neutron spectral functions for the case of three-body nuclei, which is the focus of the present study, and illustrate the shapes and magnitudes of the on-shell and off-shell smearing functions for specific models. In general, the spectral function is defined to give the probability distribution for finding a nucleon with momentum $\boldsymbol{p}$ and energy ε in the nucleus A, summed over all possible configurations of the residual $A-1$ system. For the proton spectral function in ^{3}He there are two contributions: one from the bound pn intermediate state corresponding to a deuteron, with energy $\varepsilon = \varepsilon_d - \varepsilon_{^3\mathrm{He}}$, where $\varepsilon_d = -2.22$ MeV and $\varepsilon_{^3\mathrm{He}} = -7.72$ MeV are the deuteron and ^{3}He binding energies, respectively, and one from the pn continuum scattering states, with off-shell energy ε,

$$\mathcal{F}_0^p(\varepsilon,\boldsymbol{p}) = \mathcal{F}_0^{p\,(d)}(\boldsymbol{p})\,\delta(\varepsilon+\varepsilon_{^3\mathrm{He}}-\varepsilon_d) + \mathcal{F}_0^{p\,(\mathrm{cont})}(\varepsilon,\boldsymbol{p}). \tag{19}$$

For the neutron, on the other hand, since there is no bound state of two protons, the spectral function contains only a contribution from the pp continuum scattering state,

$$\mathcal{F}_0^n(\varepsilon,\boldsymbol{p}) = \mathcal{F}_0^{n\,(\mathrm{cont})}(\varepsilon,\boldsymbol{p}). \tag{20}$$

Assuming isospin symmetry, the spectral functions for tritium, ^{3}H, can be obtained from those of ^{3}He simply by interchanging the proton and neutron. As is well known, however, this underestimates the triton binding energy of $\varepsilon_{^3\mathrm{H}} = -8.482$ MeV, and requires the addition of Coulomb interactions and charge-symmetry-breaking effects.

In practice, the spectral functions are typically evaluated in terms of the (positive) separation energy E, defined as the energy required to remove a single (on-shell) nucleon from the nucleus,

$$E = M_{A-1} + M - M_A, \tag{21}$$

where the mass of the spectator $A-1$ system is

$$M_{A-1} = \sqrt{E_{A-1}^2 - \boldsymbol{p}_{A-1}^2}, \tag{22}$$

with

$$E_{A-1} = M_A - p_0 = M_A - M - \varepsilon \tag{23}$$

the on-shell energy of the spectator system, and $\boldsymbol{p}_{A-1}^2 = \boldsymbol{p}^2$ in the rest frame of the nucleus. Solving Eqs. (21) and (23), we can write the energy ε in terms of the separation energy E as

$$\varepsilon = M_A - M - \sqrt{(E+M_A-M)^2 + \boldsymbol{p}^2}, \tag{24}$$

which in the nonrelativistic limit is approximated as

$$\varepsilon \approx -E - \frac{\boldsymbol{p}^2}{2(E+M_A-M)}. \tag{25}$$

For a nucleon at rest in the nucleus, $\boldsymbol{p}=0$, the energy ε is then simply the negative of the separation energy,

$$\varepsilon(\boldsymbol{p}=0) = -E. \tag{26}$$

The functions $\mathcal{F}_0^{p\,(d)}(\boldsymbol{p})$ and $\mathcal{F}_0^{p,n\,(\mathrm{cont})}$ can be determined by solving the three-body bound-state problem using one of several methods. Bissey *et al.* [48] solved the Faddeev equation using a separable approximation to the two-body nucleon-nucleon Paris potential [49], as well as the unitary pole approximation [50] to the Reid soft core (RSC) NN potential [51], and the Yamaguchi potential [52] with 7% mixing between $^3S_1$ and $^3D_1$ waves. The resulting smearing functions were used in the analysis of ^{3}He and ^{3}H structure functions in Refs. [21,22]. Schulze and Sauer (SS) [53] also solved the Faddeev equation for 18 channels using the Paris NN potential for the ground-state ^{3}He wave function [54] and projecting onto the deuteron and continuum scattering states.

In contrast, Ciofi degli Atti *et al.* pioneered [55,56] the use of the variational method using harmonic oscillator wave functions and the RSC NN interaction. Kievsky *et al.* (KPSV) [57] extended this approach, making use of a pair-correlated hyperspherical harmonic basis [58] with the AV18 NN potential, including a Coulomb interaction between protons and the Urbana IX three-body force. The KPSV and SS spectral functions were used in the analyses of spin-dependent ^{3}He structure functions in Refs. [26,27], and we will use these in the present work. Table I summarizes the average nucleon off-shell energy ε and kinetic energy $\langle\boldsymbol{p}^2\rangle/2M$ for the KPSV [57] and SS [53] models.

The on-shell smearing functions f_{ij}^N for the proton and neutron in ^{3}He, as well as the off-shell functions $\widetilde{f}_{ij}^N$, are illustrated in Figs. 1 and 2, respectively, for the KPSV model, at several values of the parameter γ. The diagonal functions f_{22}^N and f_{LL}^N are steeply peaked around $y=1$, but become broader with increasing γ. This has the effect of introducing stronger nuclear smearing at low values of Q^2 and at large x, where the cross sections are small, than at lower x, where they are larger. Note that for $\gamma=1$ the f_{22}^N and f_{LL}^N distributions are

TABLE I. Average nucleon energy ε and kinetic energy $\langle\boldsymbol{p}^2\rangle/2M$ (in units of MeV) in ^{3}He and ^{3}H nuclei, for the KPSV [57] and SS [53] models of the nuclear spectral functions.

Model	Nucleus	$\langle\varepsilon\rangle$	$\langle\boldsymbol{p}^2\rangle/2M$
KPSV	^{3}He	−64.28	48.85
	^{3}H	−66.56	48.84
SS	^{3}He	−53.66	38.45
	^{3}H	−55.94	38.44

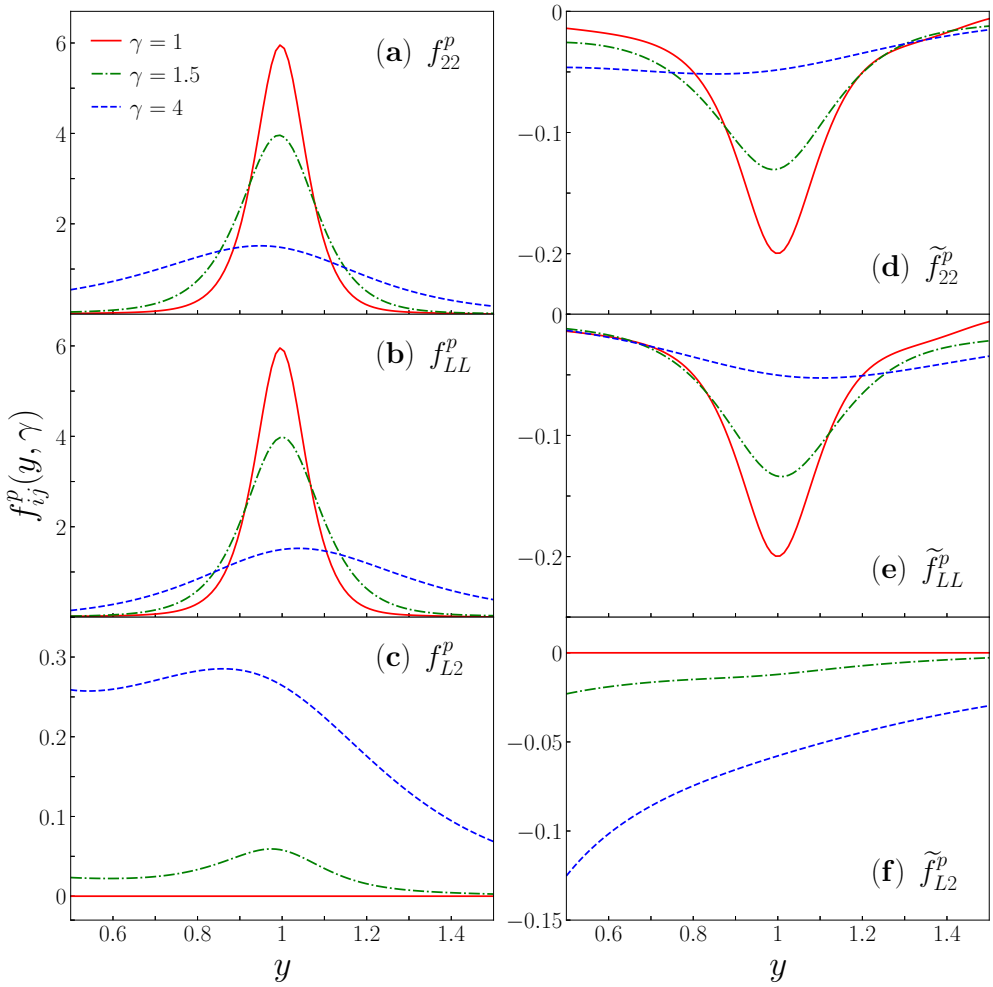

FIG. 1. Proton smearing functions in ^{3}He, $f_{ij}^p(y,\gamma)$, $i = 2, L$, for the on-shell [(a)–(c)] and off-shell [(d)–(f)] distributions, computed from the KPSV spectral function [57] for $\gamma = 1$ (red solid curves), 1.5 (green dot-dashed curves), and 4 (blue dashed curves).

identical but differ for $\gamma > 1$. The nondiagonal functions f_{L2}^N vanish identically for $\gamma = 1$, but rise to ∼20% of the diagonal functions at $y = 1$ for $\gamma = 4$.

For the off-shell smearing functions in Figs. 1 and 2, because of the factor v (<0) in the integrand of Eq. (16), these are negative for both the proton and neutron. For $\gamma = 1$, the off-shell functions $\widetilde{f}_{22}^N$ and $\widetilde{f}_{LL}^N$ are identical, with a magnitude of ≈3% of their on-shell counterparts at the peak $y \sim 1$ for the proton and ≈5% for the neutron. As for the on-shell functions, the off-shell distributions become broader with increasing γ, approximately tracking the γ dependence of the on-shell distributions.

The slightly narrower peak for the proton function in Fig. 1 compared with the neutron in Fig. 2 reflects the presence of the bound deuteron spectator contribution in the former but not in the latter. In fact, the deuteron bound-state component amounts to around 2/3 of the strength of the proton on-shell smearing function, with the continuum contribution accounting for ≈1/3. This is illustrated in Figs. 3(a) and 3(b), where the deuteron contribution is shown relative to the total for the proton on-shell f_{22}^p and off-shell $\widetilde{f}_{22}^p$ functions, respectively. For the proton off-shell function, the fraction at the $y \approx 1$ peak is closer to 1/2. Away from the peak, the deuteron pole fractions decrease rapidly for $\gamma = 1$ but remain broader for larger γ. The results for the f_{LL}^p and $\widetilde{f}_{LL}^p$ functions are very similar to those in Fig. 3, as are the ratios for the neutron.

The dependence of the smearing functions on the choice of model for the $A = 3$ wave function is illustrated in Figs. 3(c) and 3(d) as a ratio of SS [53] to KPSV [57] spectral functions for the proton f_{22}^p and $\widetilde{f}_{22}^p$ distributions. The on-shell smearing function for the SS model is slightly narrower around $y \approx 1$, with an ≈5% higher peak, which is compensated by lower distributions away from the peak. For the off-shell function, the SS model distribution is ≈5% lower than for the KPSV model, with a similar behavior away from the peak. These results illustrate an interesting compensation for the differences between the on-shell smearing functions around $y = 1$ and the off-shell functions for the two models.

With these distributions, one can now proceed to compute the nuclear structure functions F_i^A for $A =$ ^{3}He and ^{3}H, which will be the subject of the remaining sections.

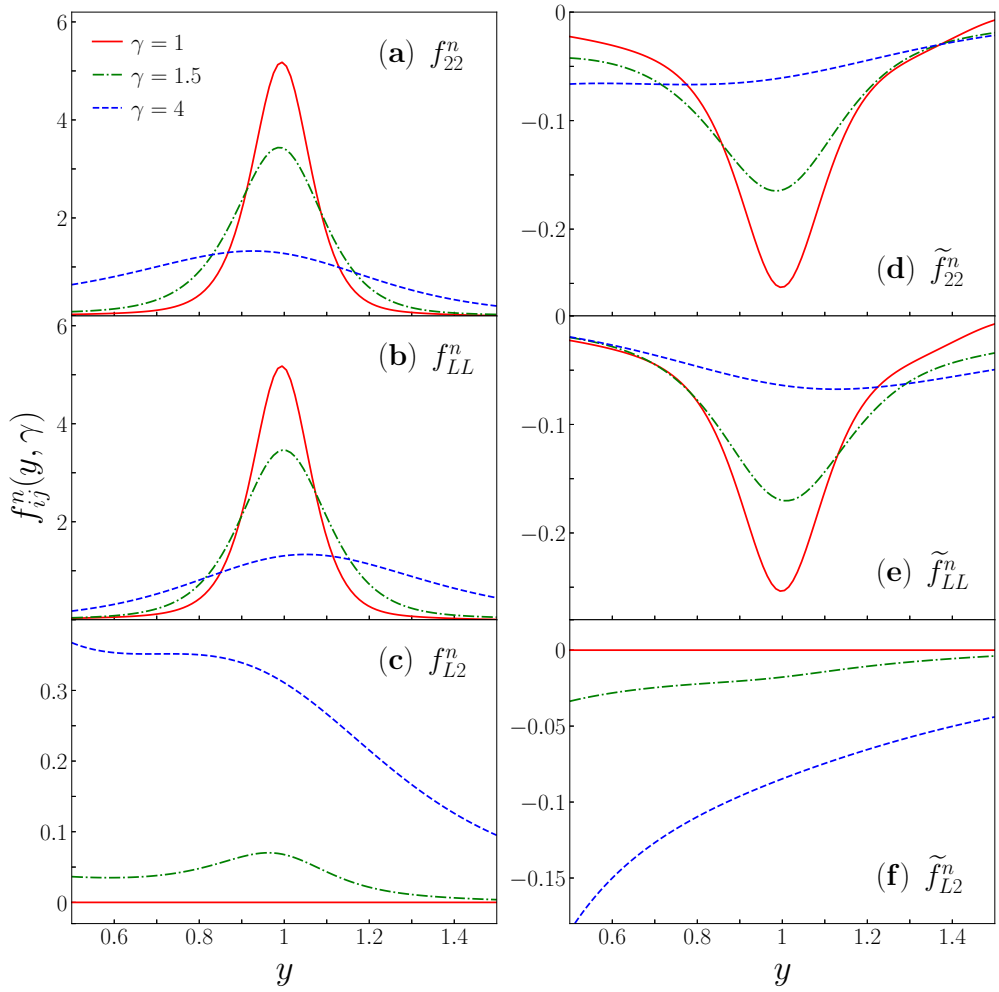

FIG. 2. Neutron smearing functions in ^{3}He, $f^n_{ij}(y,\gamma)$, $i = 2, L$, for the on-shell [(a)–(c)] and off-shell [(d)–(f)] distributions, computed from the KPSV spectral function [57] for $\gamma = 1$ (red solid curves), 1.5 (green dot-dashed curves), and 4 (blue dashed curves).

III. QUASIELASTIC SCATTERING

The veracity of any calculation of nuclear structure functions depends, within the convolution framework of Eqs. (12) and (15), on the reliability of the smearing functions $f^N_{ij}(y,\gamma)$ that characterize the distribution of nucleons in the nucleus. One of best testing grounds for models of the smearing functions is QE electron-nucleus scattering, where an electron scatters elastically from a proton or neutron bound in the nucleus. Whereas for inelastic scattering from the bound nucleon the light-cone distributions are convoluted with a nontrivial x distribution in the inelastic F^N_i structure functions, for QE scattering the cross section and structure functions are given directly by products of f^N_{ij} and Q^2-dependent elastic nucleon form factors. It is important, therefore, to establish the range of kinematics whereby the inclusive cross sections can be described in terms of the *same* smearing functions in both the deep-inelastic and QE regions. After providing the basic formulas for the QE contributions to the nuclear structure functions, in this section we compare the results for the ^{3}He cross sections with precision QE data from SLAC and Jefferson Lab in the vicinity of $x \approx 1$.

A. Quasielastic structure functions

The matrix elements of the electromagnetic current operator J^μ between on-shell nucleon states are usually parametrized in terms of the nucleon's Dirac F_{1N} and Pauli F_{2N} form factors,

$$\langle N(p+q)|J^\mu|N(p)\rangle = \bar{u}(p+q)\left[\gamma^\mu F_{1N}(Q^2) + i\sigma^{\mu\nu}q_\nu \frac{F_{2N}(Q^2)}{2M}\right]u(p). \quad (27)$$

Using the Dirac equation, and defining the Sachs electric G_{EN} and magnetic G_{MN} form factors such that

$$F_{1N}(Q^2) = \frac{1}{1+\tau}[G_{EN}(Q^2) + \tau G_{MN}(Q^2)], \quad (28a)$$

$$F_{2N}(Q^2) = \frac{1}{1+\tau}[G_{MN}(Q^2) - G_{EN}(Q^2)], \quad (28b)$$

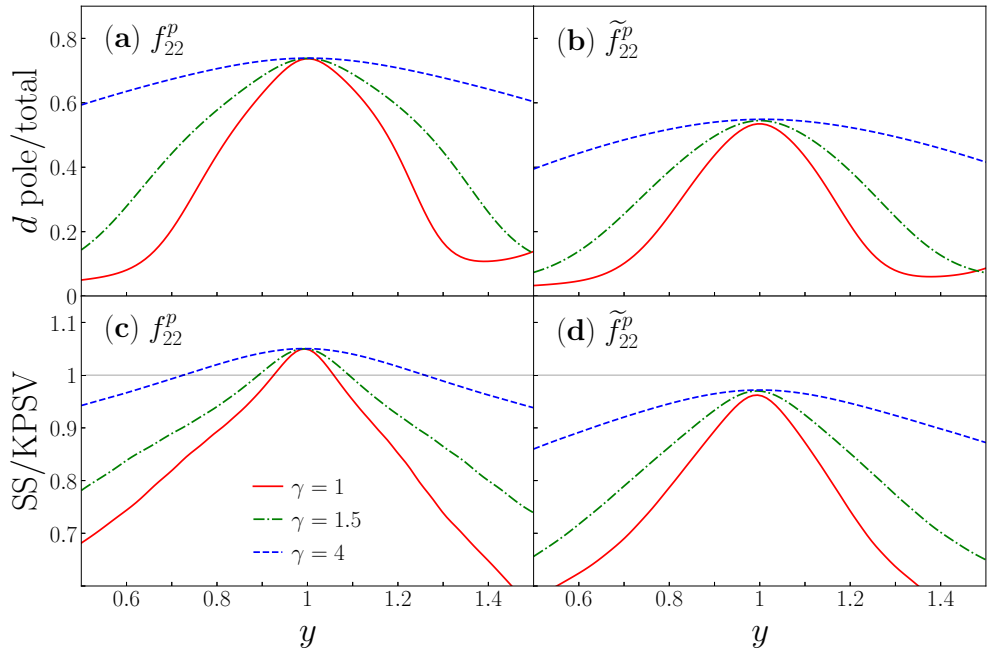

FIG. 3. Ratio of deuteron pole contribution to the total smearing function for (a) the proton on-shell f_{22}^p function and (b) proton off-shell $\widetilde{f}_{22}^p$ function, for different values of γ. The ratio of the total proton smearing functions for the SS [53] and KPSV [57] spectral functions is given in panels (c) and (d) for the on-shell and off-shell functions, respectively.

where $\tau = 4M^2/Q^2$, the matrix element can be equivalently written as

$$\langle N(p+q)|J^\mu|N(p)\rangle = \bar{u}(p+q)\left[\gamma^\mu\, G_{MN}(Q^2) \;-\; (2p^\mu + q^\mu)\frac{F_{2N}(Q^2)}{2M}\right]u(p). \tag{29}$$

The contributions to the nucleon elastic structure functions F_i^N are then given by products of the form factors multiplied by an energy conserving δ function at $x = 1$,

$$F_1^{N(\mathrm{el})}(x, Q^2) = \left[\frac{1}{2}G_{MN}^2(Q^2)\right]\delta(1-x), \tag{30a}$$

$$F_2^{N(\mathrm{el})}(x, Q^2) = \left[\frac{G_{EN}^2(Q^2) + \tau G_{MN}^2(Q^2)}{1+\tau}\right]\delta(1-x), \tag{30b}$$

where we have used the on-shell relation

$$Q^2\,\delta((p+q)^2 - M^2) = 2p\cdot q\,\delta((p+q)^2 - M^2) = \delta(1-x). \tag{31}$$

The elastic contribution to the longitudinal structure function, $F_L^{N(\mathrm{el})}$, can then be computed from Eqs. (30) using the relation $F_L^{N(\mathrm{el})}(x, Q^2) = (1 + 1/\tau)F_2^{N(\mathrm{el})}(x, Q^2) - 2F_1^{N(\mathrm{el})}(x, Q^2)$. Putting these results together, the QE nuclear structure functions can be written in terms of the nucleon Sachs form factors as

$$xF_1^{A(\mathrm{QE})}(x, Q^2) = \sum_N \left\{\frac{1}{2}x f_{11}^N(x,\gamma)\, G_{MN}^2(Q^2) \;+\; x f_{12}^N(x,\gamma) \times \left[\frac{G_{EN}^2(Q^2) + \tau G_{MN}^2(Q^2)}{1+\tau}\right]\right\}, \tag{32a}$$

$$F_2^{A(\mathrm{QE})}(x, Q^2) = \sum_N x f_{22}^N(x,\gamma)\left[\frac{G_{EN}^2(Q^2) + \tau G_{MN}^2(Q^2)}{1+\tau}\right]. \tag{32b}$$

B. Off-shell nucleons

Generalizing to the case where the struck nucleon is bound inside a nucleus, and hence off its mass shell, $p^2 \neq M^2$, one can write the kinematic constraint for elastic scattering to an on-shell nucleon final state as $2p\cdot q = Q^2 + M^2 - p^2 = Q^2/(x/y)$, where y is defined in Eq. (8). In this case, the δ function in Eq. (31) can be written as

$$Q^2\,\delta((p+q)^2 - M^2) = \frac{x}{y}\,\delta\left(1 - \kappa(p^2)\,\frac{x}{y}\right), \tag{33}$$

where $\kappa(p^2) = 1 - v(p^2)\,M^2/Q^2$ parametrizes the kinematical effects of the off-shell correction. The generalization of the current operator to off shell is not unique, and in the literature one encounters several prescriptions for this. The most common ones are the "cc1" and "cc2" prescription of De Forest [59], which correspond to generalizing the currents in Eqs. (29) and (27), respectively, to the off-shell region. The

elastic structure functions for the off-shell nucleon are then given by

$$\widetilde{F}_1^{N(\mathrm{el})}\left(\frac{x}{y}, Q^2, p^2\right) = \left[\frac{G_{MN}^2}{2}\left(1+\frac{\upsilon M^2}{Q^2}\right)\right]\frac{x}{y}\delta\left(1-\kappa(p^2)\,\frac{x}{y}\right), \tag{34a}$$

$$\widetilde{F}_2^{N(\mathrm{el})}\left(\frac{x}{y}, Q^2, p^2\right) = \left[\frac{G_{EN}^2+\tau G_{MN}^2}{1+\tau} + \upsilon\,\frac{(G_{MN}-G_{EN})^2}{4(1+\tau)^2}\right] \times \delta\left(1-\kappa(p^2)\,\frac{x}{y}\right), \tag{34b}$$

and

$$\widetilde{F}_1^{N(\mathrm{el})}\left(\frac{x}{y}, Q^2, p^2\right) = \left[\frac{G_{MN}^2}{2} + \frac{\upsilon M^2}{2Q^2}\left(\frac{G_{EN}^2+\tau G_{MN}^2}{1+\tau} + \upsilon\,\frac{(G_{MN}-G_{EN})^2}{4(1+\tau)^2}\right)\right] \times \frac{x}{y}\delta\left(1-\kappa(p^2)\,\frac{x}{y}\right), \tag{35a}$$

$$\widetilde{F}_2^{N(\mathrm{el})}\left(\frac{x}{y}, Q^2, p^2\right) = \left[\frac{G_{EN}^2+\tau G_{MN}^2}{1+\tau}\right]\delta\left(1-\kappa(p^2)\,\frac{x}{y}\right), \tag{35b}$$

for the "cc1" and "cc2" cases, respectively. Assuming the G_E and G_M form factors themselves remain functions of Q^2 only, the off-shell corrections to the on-shell elastic structure functions in Eqs. (30) involve terms that are of order υ and υ^2, in addition to the modified δ function. In each case, the off-shell corrections vanish in the $Q^2 \to \infty$ limit. In terms of the elastic off-shell functions, the total QE structure functions can be computed by substituting Eqs. (34) or (35) into Eqs. (7), and using the δ function in Eq. (33) to eliminate the dy integration in $d^4p \to dy\, d|\boldsymbol{p}|\, d\varepsilon$, so that the QE structure functions are computed as integrals over the variables $|\boldsymbol{p}|$ and ε. Alternatively, one can use the δ function to eliminate the $|\boldsymbol{p}|$ or p^2 integration, leaving integrations over ε and y.

In the following, we discuss the off-shell corrections numerically and compare the WBA predictions for the QE cross sections with experimental measurements of the inclusive cross sections in the QE region at $x \sim 1$.

C. Comparison with quasielastic ^{3}He data

A number of experiments have been performed scattering electrons from $A = 3$ nuclei in the QE region, over a range of energies and scattering angles. A convenient summary of the experimental data is provided in the Quasielastic Electron-Nucleus Scattering Archive [60]. The most relevant of these for the present analysis are data from experiments at SLAC [35,36] and Jefferson Lab [37].

The early SLAC data from Ref. [35] were taken for incident electron energies between 3 and 15 GeV at $\theta = 8^\circ$ scattering angle, corresponding to momentum transfers of up to ≈1.4 GeV. Measurements from the subsequent NE9 experiment [36] were taken at electron energies between 0.9 and 4.3 GeV, and scattering angles of 15° and 85°. Both the transverse and longitudinal structure functions were extracted using the Rosenbluth separation technique at a three-momentum transfer of ≈1 GeV, and the latter was used to test the Coulomb sum rule. More recently, high-precision data from the Jefferson Lab experiment E02-019 were collected using a 5.766-GeV electron beam on various nuclear targets, including ^{3}He, primarily to study "superfast" quarks at $x > 1$ [37]. QE data were taken at scattering angles between 18° and 50°, corresponding to values of the four-momentum exchange squared of $2 \lesssim Q^2 \lesssim 9$ GeV^2.

Data from lower energy experiments from Bates [61] and Saclay [62], on ^{3}He as well as ^{3}H targets, are not included in our analysis, which focuses on the region of validity of the nuclear impulse approximation, corresponding to intermediate Q^2 values from ≈1 GeV^2 to a few GeV^2. At very large values of $x \gg 1$, contributions from processes involving nucleons that no longer retain their clear identity as nonoverlapping bound states of quarks, as well as multinucleon effects requiring nuclear quark degrees of freedom, are expected to become more important. At very low Q^2 values, $Q^2 \ll 1$ GeV^2, coherent effects and meson exchange corrections, as well as rescattering, are known to play a greater role. At higher Q^2 values, $Q^2 \gg 1$ GeV^2, identification of the QE component of the inclusive cross section underneath the rising inelastic scattering contributions becomes increasingly more difficult and model dependent. In the $Q^2 \sim 1$ GeV^2 to several GeV^2 range, where the $x \sim 1$ region should still be dominated by single-nucleon QE scattering, one can explore the efficacy and limitations of an incoherent impulse approximation description in terms of the nucleon smearing functions of Sec. II.

In Fig. 4, the QE data from the SLAC experiments [35,36] are compared with the cross sections computed from the smearing functions in the WBA model. The data include both forward scattering angles [Figs. 4(a)–4(d) and 4(f)], as well as sideways scattering [Fig. 4(e)], with the value of Q^2 at $x = 1$ (labeled by Q_0^2) ranging from ≈1 GeV^2 to ≲4 GeV^2. For the elastic structure function, we use the parametrizations of the electric and magnetic form factors of the proton and neutron from Kelly [63]. Experience from previous analyses of QE scattering from the deuteron [64] shows that use of other parametrizations, e.g., those from Refs. [65–67], has little (≲ few %) effect on the cross sections at the relavant kinematics.

As a baseline for the calculation, the KPSV [57] model is used for the ^{3}He spectral function, and the results with and without the off-shell corrections are compared. As Fig. 4 illustrates, the effect of the off-shell corrections is a softening of the momentum distribution, which shifts the peak in the cross section to slightly lower values of x and improves the overall agreement with the data. The difference between the off-shell corrections computed using the two prescription ("cc1" or "cc2") is very small, and, as expected from Eqs. (33)–(35), the off-shell effects become less prominent with increasing Q^2.

The importance of the Q^2 dependence is illustrated more strikingly in Figs. 4(a) and 4(d), which compares the calculation using exact kinematics with that taking smearing functions at $\gamma = 1$, as often done in deep-inelastic scattering applications at high Q^2. The result with $\gamma = 1$ gives a significantly narrower distribution around $x = 1$, and a peak that is

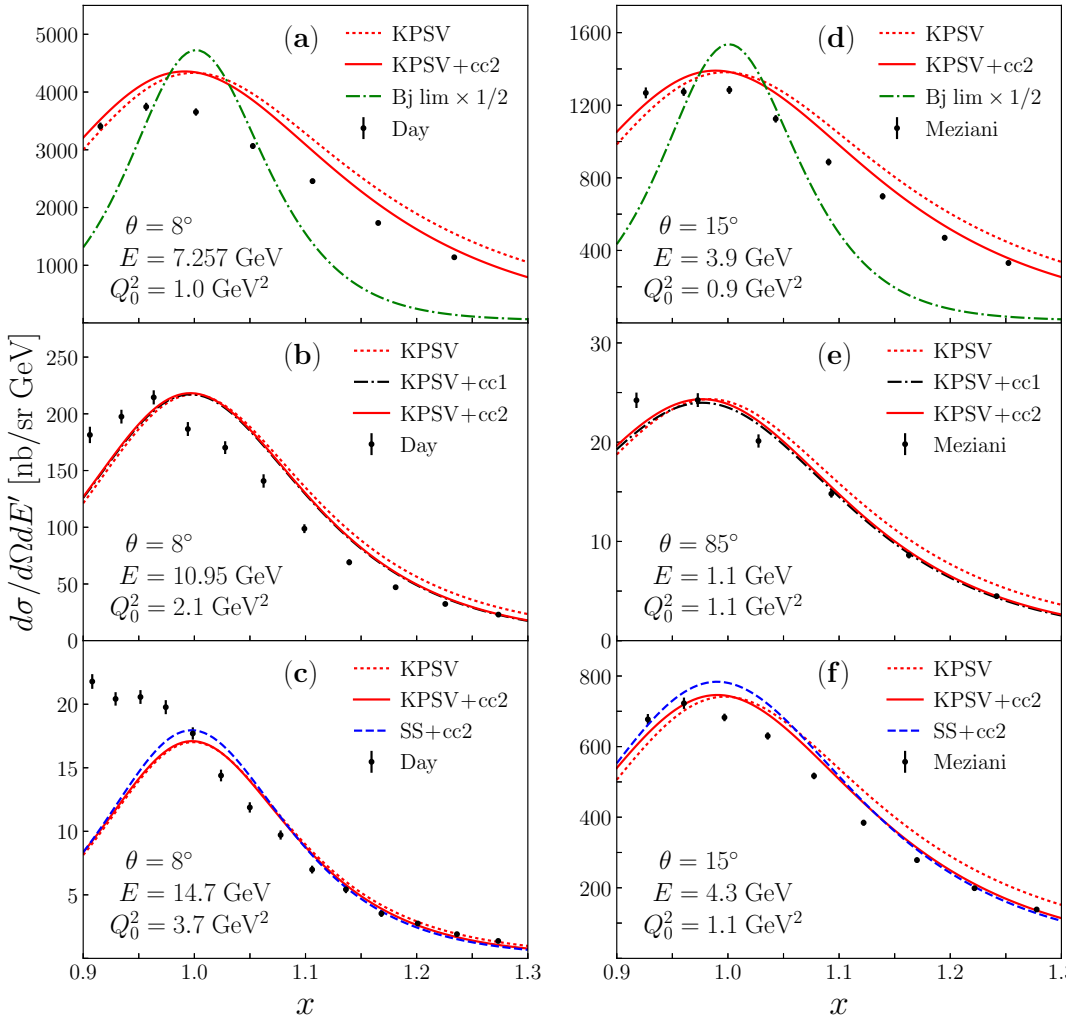

FIG. 4. QE electron-^{3}He cross section as a function of x for fixed incident electron energies E and scattering angles θ, with Q_0^2 the value of the momentum transfer squared at $x = 1$. Data from the early SLAC experiment by Day *et al.* [35] [(a)–(c)] and the subsequent NE9 experiment by Meziani *et al.* [36] [(d)–(f)] are compared with the WBA calculation using the KPSV and SS spectral functions, and the "cc1" and "cc2" off-shell prescriptions, as well as a calculation using smearing functions at $\gamma = 1$ [(a) and (d)], scaled by a factor $1/2$ for clarity.

≈2 times larger than the data indicate. In contrast, the results with the finite-Q^2 kinematics correctly implemented is in significantly better agreement with the data. The dependence of the results on the ^{3}He spectral function is very mild, as the comparison with the SS spectral function [53] in Figs. 4(c) and 4(f) shows, with the SS results giving a slightly narrower distribution around the QE peak compared with the KPSV spectral function [57].

Overall, the qualitative features of the data versus theory comparisons are similar for the Day *et al.* [35] and Meziani *et al.* [36] data, with the agreement being somewhat better for the more recent data set [36]. The similar kinematics of the two experiments, in particular for forward scattering angles at $Q^2 \sim 1$ GeV^2, raise the question of whether there may be a systematic underestimate in the Day *et al.* [35] data in this region.

The most recent QE data from Jefferson Lab experiment E02-019 [37] are shown in Fig. 5, for a fixed electron energy $E = 5.766$ GeV and scattering angles from $\theta = 18^\circ$ to 50°. This corresponds to slightly larger Q^2 values at the QE peak than for the SLAC data in Fig. 4, ranging from $Q_0^2 \approx 2.5$ GeV^2 to ≈7.4 GeV^2. At these higher Q^2 values the effects of the off-shell corrections are relatively small, and for the spectra with $Q_0^2 \gtrsim 4$ GeV^2 the full cross sections are almost indistinguishable from the on-shell-only contributions.

What is rather more important at the higher Q^2 values are the effects of the inelastic scattering contributions. These are illustrated in Fig. 5(e) at $Q_0^2 \approx 6.3$ GeV^2 and Fig. 5(f) at $Q_0^2 \approx 7.4$ GeV^2, using the nonresonant part of the Christy-Bosted nucleon structure function parametrization [68]. For the higher Q_0^2 case in particular, the inelastic cross section is quite large—more than half of the total at the QE peak—and dominates at smaller x values, $x \lesssim 1$.

Since the inelastic contribution in the present work is not fitted but simply ported from a previous phenomenological analysis [68], and since the separation of the total cross section into resonance and nonresonant contributions is not unique, achieving quantitative agreement of the QE plus inelastic

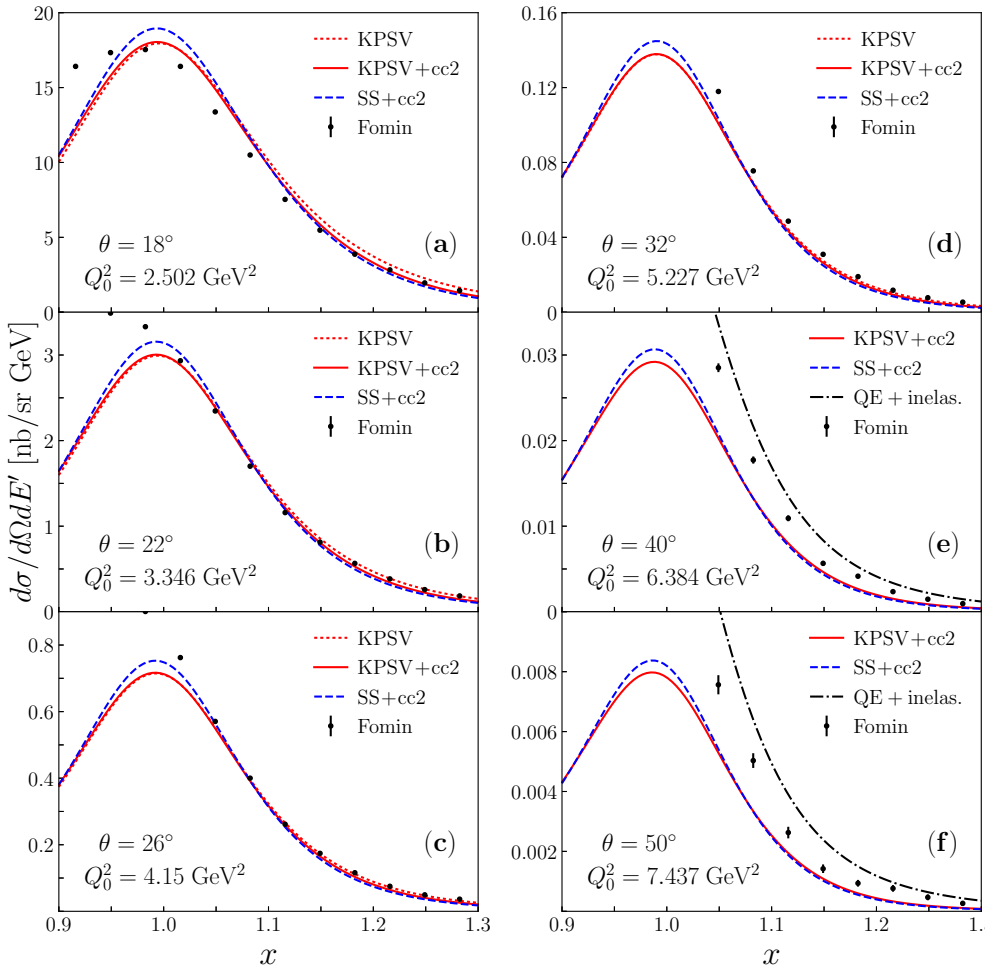

FIG. 5. As in Fig. 4, but for the Jefferson Lab QE data from Fomin *et al.* [37] at $E = 5.766$ GeV. Cross sections which include inelastic contributions are illustrated in panels (e) and (f) (black dot-dashed curves).

sum with the data is not the primary goal. The points to be noted in this comparison are the relative magnitude of the inelastic component compared with the nucleon elastic and the difficulty in determining the QE piece unambiguously at high values of Q^2, especially for $Q_0^2 \gtrsim 4 - 5$ GeV^2.

The dependence on the model ^{3}He spectral function is similar to that in Fig. 4, with the SS model [53] giving a slightly higher cross section at $x \approx 1$, with marginally softer distributions away from the QE peak. Overall, the agreement with the data is relatively good for both spectral function models and suggests that at these kinematics the description in terms of the smearing functions, with indications of small but nonzero off-shell corrections, can provide a reliable framework for describing electron scattering from ^{3}He. The agreement of the calculation with the data at kinematics $Q_0^2 \approx 2$ GeV^2 comparable to some of the Day *et al.* spectra again suggests potential issues with these data.

In the near future, the recently completed Jefferson Lab E12-11-112 experiment [38] will provide additional information on QE scattering in the $Q^2 \sim$ 1–3 GeV^2 for both ^{3}He and ^{3}H nuclei. An estimate of the anticipated cross sections at the E12-11-112 kinematics is given in Fig. 6, for a beam energy of $E = 4.3$ GeV and scattering angles of 15° and 30°. Interestingly, the ^{3}He cross section at the QE peak is ≈30–40% larger than the corresponding ^{3}H cross section, which can be understood from the larger elastic contribution to the proton structure function compared with the neutron, $F_2^{p\,(\mathrm{el})} > F_2^{n\,(\mathrm{el})}$, which is doubly represented in ^{3}He. The wave function model dependence is again relatively weak, as Fig. 6 illustrates with the ratios of the ^{3}He to ^{3}H cross sections. Confronting these predictions with the E12-11-112 data will provide important guidance for the identification of isospin-dependent effects in scattering from $A = 3$ nuclei, and the limitations of the impulse approximation and the WBA framework for computing the smearing functions.

D. Elastic form factors from QE data

If the ^{3}He and ^{3}H smearing functions are sufficiently well constrained at $y \approx 1$, the QE ^{3}He and ^{3}H data can also be used to extract information about the nucleon's elastic electromagnetic form factors. In particular, from the ratio of ^{3}He to ^{3}H QE cross sections measured in the E12-11-112 experiment [38] at $x = 1$ and input on the proton's electromagnetic form factors and the neutron's electric form factor,

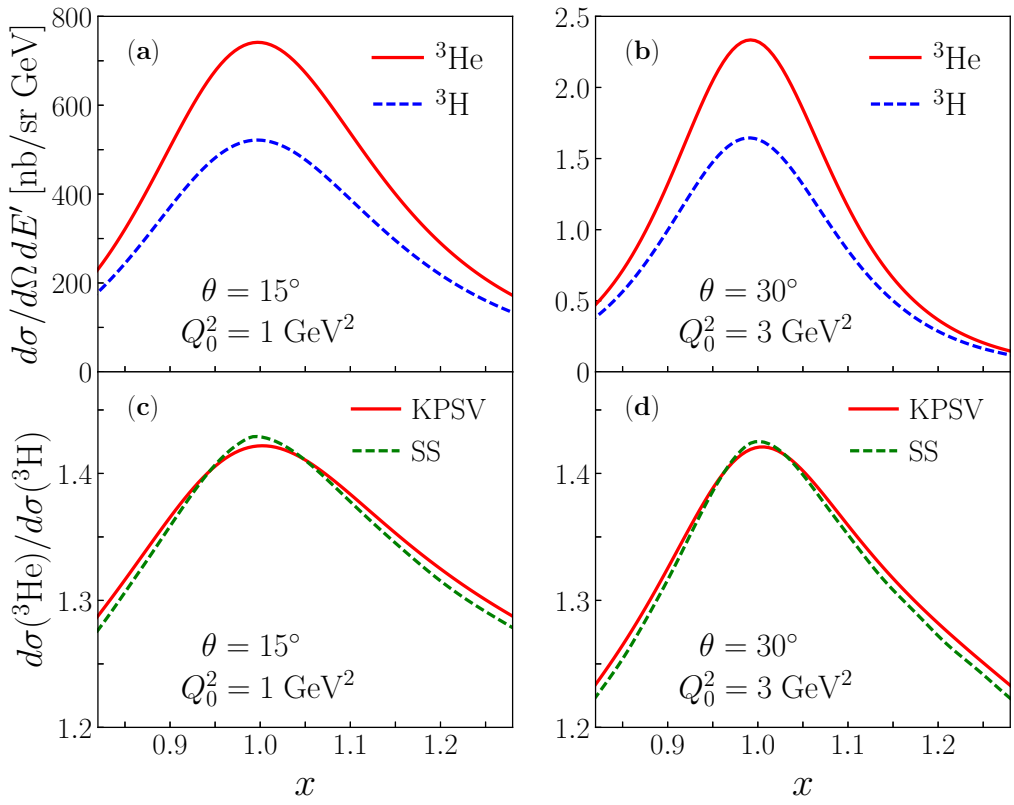

FIG. 6. QE cross section for ^{3}He (red solid curves) and ^{3}H (blue dashed curves) [in units of nb/sr GeV] at typical kinematics of the E12-11-112 experiment [38] with $E = 4.3$ GeV, for (a) $\theta = 15°$ and $Q_0^2 = 1$ GeV^2 and (b) $\theta = 30°$ and $Q_0^2 = 3$ GeV^2. The corresponding ratios of the ^{3}He and ^{3}H cross sections in panels (c) and (d) illustrate the effects of the different $A = 3$ spectral functions, from the KPSV (red solid curves) and SS (green dashed curves) models.

one can in principle extract the free neutron's magnetic form factor, G_{Mn}.

A simple inversion of the QE formulas in the on-shell approximation in Eqs. (32) allows the nucleon elastic form factors G_{EN}, G_{MN} to be determined from the smearing functions f_{ij}^N and the ^{3}He to ^{3}H structure functions. To maximize the rates and simplify the analysis, one can take the QE cross section in the vicinity of the QE peak, $x \approx 1$. Taking the F_2 structure function as an example, the ratio of the QE ^{3}He to ^{3}H functions can then be written as

$$R^{(\mathrm{QE})} \equiv \frac{F_2^{^3\mathrm{He(QE)}}}{F_2^{^3\mathrm{H(QE)}}} = \frac{2 + (f^n/f^p) R_{np}}{(f^n/f^p) + 2R_{np}}, \tag{36}$$

where $f^N \equiv f_{22}^N(x = 1, \gamma)$ and

$$R_{np} = \frac{G_{En}^2 + \tau G_{Mn}^2}{G_{Ep}^2 + \tau G_{Mp}^2} \tag{37}$$

is the ratio of the neutron to proton form factor combination entering the F_2 structure function. From Figs. 1 and 2, the ratio of the neutron to proton smearing functions at $y = 1$ is $\approx$0.87, almost independent of γ for the range $\gamma = 1$–4 considered there, for both the KPSV and SS spectral function models. The weak model dependence of the ratio is also illustrated in the QE ^{3}He to ^{3}H cross-section ratio in Fig. 6, which is $\approx$1.4 at the QE peak.

Note that a slightly different combination of form factors would be extracted from ratios of the QE $F_1^{A(\mathrm{QE})}$ structure functions, or from ratios of the actual cross sections, which are combinations of $F_1^{A(\mathrm{QE})}$ and $F_2^{A(\mathrm{QE})}$. In practice, this would be immaterial, as one could either extract $F_1^{A(\mathrm{QE})}$ and $F_2^{A(\mathrm{QE})}$ from the cross section by performing a Rosenbluth separation, or simply work in terms of a different combination of the G_{EN} and G_{MN} form factors which enters the cross section.

Inverting Eq. (36), one can write the form factor ratio in Eq. (37) as

$$R_{np} = \frac{(f^n/f^p) R^{(\mathrm{QE})} - 2}{(f^n/f^p) - 2R^{(\mathrm{QE})}}, \tag{38}$$

with the QE ratio $R^{(\mathrm{QE})}$ defined as in Eq. (36). Measurement of $R^{(\mathrm{QE})}$, together with a model for the smearing function ratio f^n/f^p and knowledge of G_{Ep}, G_{Mp}, and G_{En}, can then be used to infer the magnetic neutron form factor G_{Mn}. In Fig. 7, we show the ratio of G_{Mn} extracted from Eq. (38) to the input parametrization, $G_{Mn}^{(0)}$. The full calculation, illustrated here for the on-shell nucleon structure function case with proton and neutron electromagnetic form factors from Ref. [63], of course gives a ratio of unity, reflecting the self-consistency of the extraction method. In contrast, if one were to use Eq. (38) with the assumption $f^p = f^n$, the extracted G_{Mn} would be $\approx$10% lower over the range $Q^2 \approx 1$–8 GeV^2 than the true result. Similar results are found for the off-shell calculation,

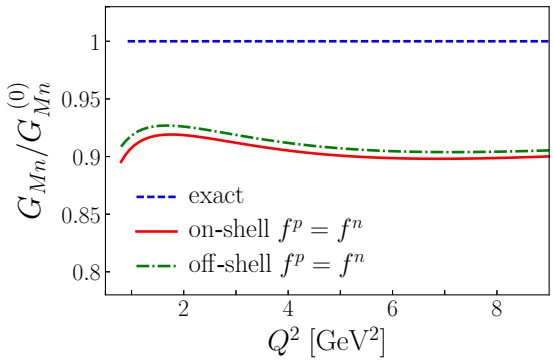

FIG. 7. Ratio of the neutron magnetic form factor G_{Mn}, extracted from Eqs. (37) and (38), to the input form factor $G_{Mn}^{(0)}$ taken from the Kelly parametrization [63]. The extracted G_{Mn} is computed using the exact on-shell calculation (dashed blue curve), giving a ratio of unity, and with G_{Mn} computed from Eq. (38) but with $f^p = f^n$ (solid red curve), or for $f^p = f^n$ with the off-shell calculation using the "cc2" prescription (dot-dashed green curve).

as illustrated in Fig. 7 for the "cc2" prescription. Therefore, if one seeks experiments with precision for the extracted G_{Mn} to less than $\approx$10% at these kinematics, using the correct smearing function ratios would clearly be important in such analyses.

IV. DEEP-INELASTIC SCATTERING FROM ^{3}He AND ^{3}H

The central motivation for the MARATHON experiment [20] at Jefferson Lab is the measurement of the inclusive ^{3}He to ^{3}H cross-section ratio in the deep-inelastic scattering region, from which one hopes to extract the ratio of the free neutron to proton structure functions [21–24]. At large values of x ($x \gtrsim 0.6$), poor knowledge of the neutron structure function has prevented a reliable determination of the d/u quark PDF ratio in the proton from inclusive DIS data [5]. Assuming that contributions from the scattering of longitudinal photons are either sufficiently small or can be accurately estimated, the ratio of the cross sections (4) for ^{3}He and ^{3}H can be used to determine the $F_2^{^3\mathrm{He}}/F_2^{^3\mathrm{H}}$ structure function ratio, from which F_2^n/F_2^p can be extracted via [21–24]

$$\frac{F_2^n}{F_2^p} = \frac{2\mathcal{R} - F_2^{^3\mathrm{He}}/F_2^{^3\mathrm{H}}}{2F_2^{^3\mathrm{He}}/F_2^{^3\mathrm{H}} - \mathcal{R}}, \tag{39}$$

where

$$\mathcal{R} = \frac{R(^3\mathrm{He})}{R(^3\mathrm{H})} \tag{40}$$

is the "super-ratio" of nuclear EMC ratios in ^{3}He and in ^{3}H,

$$R(^3\mathrm{He}) = \frac{F_2^{^3\mathrm{He}}}{2F_2^p + F_2^n}, \tag{41a}$$

$$R(^3\mathrm{H}) = \frac{F_2^{^3\mathrm{H}}}{F_2^p + 2F_2^n}. \tag{41b}$$

Without a direct measurement of F_2^n, the EMC ratios $R(^3\mathrm{He})$ and $R(^3\mathrm{H})$ themselves cannot be uniquely determined. However, irrespective of the magnitude of the nuclear corrections in either ^{3}He or ^{3}H, if these effects are similar in the mirror nuclei or can be reliably determined theoretically, then the uncertainty introduced in the extraction of F_2^n/F_2^p in Eq. (39) due to the super-ratio $\mathcal{R}$ can be minimized.

Several previous studies have estimated the super-ratio within various nuclear models. Among the standard approaches based on the impulse approximation, Pace *et al.* [23] used a convolution framework similar to that in Sec. II, together with smearing functions computed in a correlated hyperspherical harmonics basis, including Coulomb and three-body interactions. Afnan *et al.* [21,22] evaluated the super-ratio in the convolution approximation using three-nucleon wave functions obtained by solving the Faddeev equation, as well as using the variational approach, while Sargsian *et al.* [24] employed a virtual-nucleon convolution model in addition to a model based on light-front kinematics. All these estimates found deviations of $\mathcal{R}$ of $\lesssim$1–2% from unity over the range accessible in the MARATHON experiment.

Beyond the impulse approximation, Afnan *et al.* [22] considered the impact on the super-ratio of off-shell corrections computed from a spectator quark model [42,69], as well as from six-quark clusters, and a commonly used ansatz based on nuclear density scaling [70]. Sargsian *et al.* [24] further considered a Q^2 rescaling model of the nuclear EMC effect [71,72] and a color screening model in which off-shell effects were represented in the form of short-range NN correlations [70]. To estimate the effect of possible isospin dependence of the NN correlation, the isosinglet and isotriplet combinations were assumed to experience different amounts of suppression. Of the scenarios considered, the isospin-dependent effects produced at most a 2–3% deviation in the super-ratio for $x \lesssim 0.8$. Of course, any evidence of stronger isospin-breaking corrections could induce larger effects on the super-ratio.

In this section, we explore whether the data on the ratio of ^{3}He to deuterium DIS cross sections from the Jefferson Lab E03-103 experiment [33], that were taken after the earlier studies [21–24] were performed, are able to provide any constraints on the possible isospin dependence of the nuclear corrections and hence $\mathcal{R}$. In particular, we examine whether any isospin dependence in the off-shell corrections to the nucleon structure functions in Eq. (10) can have noticeable effects on the super-ratio $\mathcal{R}$ and on the neutron/proton ratio extraction. Such isospin dependence would not be visible in global QCD analyses of deuterium data [15,16], but could play a role in the scattering from the isospin asymmetric ^{3}He and ^{3}H system. Moreover, as an alternative to the super-ratio method (39) described above, we also propose a more robust extraction procedure which, although requiring additional experimental inputs, does not rely on any assumptions about $\mathcal{R}$.

A. Nucleon off-shell corrections

Recently, the CJ Collaboration [15] and Alekhin *et al.* [16] performed global analyses of deuteron DIS and other high-energy scattering data in which nucleon off-shell contributions

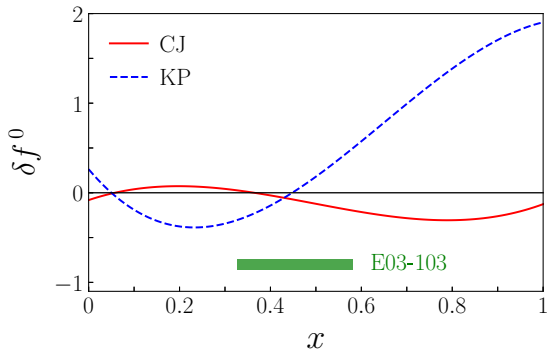

FIG. 8. Isoscalar off-shell function δf^0 from the CJ15 [15] global QCD analysis of proton and deuteron data (red solid curve) and the Kulagin-Petti (KP) [25] fit to of nuclear structure function ratios, assuming $\delta f^p = \delta f^n$. The kinematics of the Jefferson Lab E03-103 experiment [33] are indicated by the green horizontal band.

to the deuteron F_2 structure function in Eq. (15b) were obtained by fitting the isoscalar off-shell function δf^0 directly,

$$F_2^{d(\text{off})}(x) = \int dy\, \widetilde{f}_{22}^{N/d}(y,\gamma)\left[F_2^p\left(\frac{x}{y}\right) + F_2^n\left(\frac{x}{y}\right)\right]\delta f^0\left(\frac{x}{y}\right), \tag{42}$$

where δf^0 is related to the proton and neutron off-shell functions in Eq. (10) by

$$\delta f^0(x) = \frac{F_2^p(x)\,\delta f^p(x) + F_2^n(x)\,\delta f^n(x)}{F_2^p(x) + F_2^n(x)}. \tag{43}$$

(For simplicity here we have suppressed the Q^2 dependence in the structure functions.) Despite some differences in the fitted shapes of the off-shell functions in the two analyses [15,16], the overall magnitude of the off-shell effects was found to be relatively small for the isoscalar combination δf^0. Assuming isospin independence of the off-shell corrections, Kulagin and Petti (KP) [25] also fitted data on ratios of structure functions of heavy nuclei to deuterium, extracting a universal function $\delta f^N \equiv \delta f^0 = \delta f^p = \delta f^n$ that agreed with the shape of that in Ref. [16] but was somewhat larger than that from the CJ15 analysis [15].

The isoscalar off-shell functions δf^0 from the CJ15 PDF analysis [15] and from the earlier KP nuclear structure function fit [25] are shown in Fig. 8. Both analyses used a parametrization based on a third-order polynomial of the form

$$\delta f^0(x) = C(x - x_0)(x - x_1)(1 + x_0 - x), \tag{44}$$

with parameters x_0 and x_1 and normalization C, which was constructed to ensure at least one zero in the physical region of x. The CJ15 analysis further imposed the normalization [15]

$$\int_0^1 dx\, \delta f^0(x)[q(x) - \bar{q}(x)] = 0 \tag{45}$$

to ensure that the off-shell corrections do not modify the valence quark number. As Fig. 8 illustrates, the CJ analysis found a relatively small magnitude for δf^0, slightly positive at low x ($x \sim 0.2$) and negative at large x ($x \gtrsim 0.4$). The best fit corresponds to a deuteron wave function computed from the AV18 NN interaction [73], although similar quality fits were found using the CD-Bonn [74] and WJC-2 [75] wave functions, giving overall similar shapes for δf^0. In contrast, the off-shell function from the KP fit [25], which uses the Paris NN potential [76], generally has opposite sign compared with the CJ result in Fig. 8 and a somewhat larger magnitude which grows as $x \to 1$. Interestingly, in the CJ analysis, a shape similar to this was found for the WJC-1 [75] deuteron wave function, which, however, gave a slightly larger overall χ^2 value for the global fit.

While the origin of the different behaviors for δf^0 found in the two analyses is difficult to determine uniquely, one can speculate that it may arise partly from the use of heavy nuclear data in Ref. [25], which generally show a stronger nuclear EMC effect than that in lighter nuclei. To be conservative, in the present analysis we consider both scenarios and investigate the consequences for the $A = 3$ structure functions of both shapes for δf^0 shown in Fig. 8.

B. Isospin dependence of off-shell corrections

Although deuterium data can only constrain the isoscalar combination of PDFs and off-shell functions, data from the Jefferson Lab E03-103 experiment [33] on the ratio of ^{3}He to deuterium cross sections could in principle allow the isospin dependence to be disentangled. In particular, because the ^{3}He cross section is more sensitive to proton structure, one can attempt to constrain the proton δf^p correction from the ^{3}He/d ratio, and, using information from the global analyses on δf^0 [15,25], extract the neutron off-shell correction from Eq. (43),

$$\begin{aligned}\delta f^n &= \frac{1}{F_2^n}\left[\left(F_2^p + F_2^n\right)\delta f^0 - F_2^p\,\delta f^p\right] \\ &= \delta f^0 - \frac{F_2^p}{F_2^n}(\delta f^p - \delta f^0).\end{aligned} \tag{46}$$

In the remainder of this section, we will analyze the ^{3}He/d data from Seely *et al.* [33] within the theoretical framework of Sec. II, and discuss the implications of these data for the isospin dependence of the off-shell corrections.

The ^{3}He/d data from the E03-103 experiment [33] were taken in Jefferson Lab Hall C, using a 5.767-GeV beam of electrons scattering mostly to an angle of 40°. In the DIS region, $W^2 > 4$ GeV^2, the kinematics covered the range $0.33 \lesssim x \lesssim 0.58$ and $2.9 \lesssim Q^2 \lesssim 4.4$ GeV^2. The measured ratio of the ^{3}He to d cross sections is shown in Fig. 9, where the cross sections are scaled to those per nucleon (total cross-section ratio multiplied by a factor 2/3). Note that the data here do not include any "isoscalar correction," which can introduce unnecessary theoretical bias into the analysis. The experimental error bars include statistical uncertainties and point-to-point systematic uncertainties added in quadrature. In addition, there is an overall 1.84% fractional normalization uncertainty that is not shown in Fig. 9.

For the analysis of the ^{3}He/d ratio, we fit the proton off-shell function δf^p using the same parametrization as for the isoscalar off-shell function in Eq. (44). Using the maximum likelihood method with Hessian error propagation, we fit

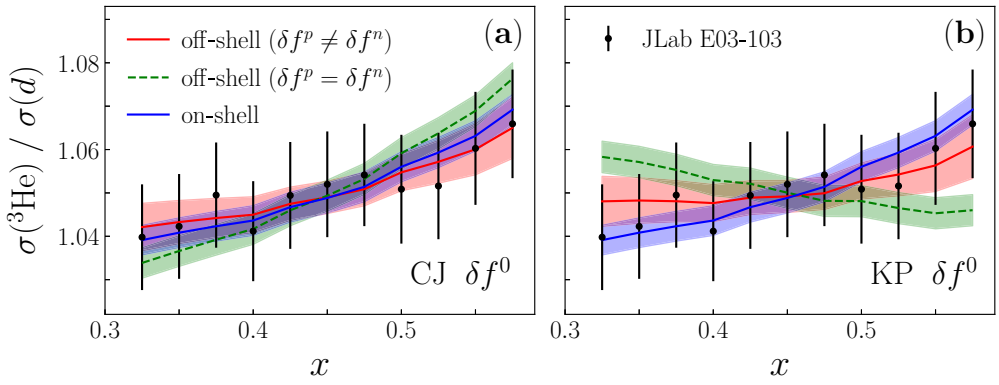

FIG. 9. Ratio of ^{3}He to deuterium cross sections, $\sigma^{^3\mathrm{He}}/\sigma^d$, scaled per nucleon, from the Jefferson Lab E03-103 experiment [33] compared with the full Monte Carlo fit results (red solid curves and bands) using (a) the CJ [15] and (b) the KP [25] isoscalar off-shell function δf^0, as well as with fits assuming isospin symmetric off-shell corrections, $\delta f^p = \delta f^n$ (green dashed curves and bands), and with the on-shell only fits (blue solid curves and bands). The experimental error bars include statistical and systematic uncertainties added in quadrature, with an overall 1.84% normalization uncertainty not shown [85].

the x-intercept x_0 and the normalization parameter C and determine the position of the zero crossing at x_1 from the off-shell normalization constraint (45). The results are found to be rather strongly dependent on the starting parameters of the fit, indicating the presence of more than a single χ^2 minimum in parameter space. To avoid this problem, we turn instead to a Monte Carlo analysis method, using the nested sampling algorithm [77–79] to map the likelihood function into a Monte Carlo weighted parameter sample. This method accounts for the possible presence of multiple minima and allows a rigorous determination of the fit uncertainties. Similar methodology was recently used by the JAM Collaboration to extract collinear PDFs [80–82] and fragmentation functions [83], as well as the transverse momentum-dependent transversity distribution [84].

The results of the Monte Carlo fit to the ^{3}He/d data in Fig. 9 for the distribution of the fitted parameters C and x_0 are shown in Fig. 10. For the CJ isoscalar function δf^0, the normalization parameter C is peaked for positive values, while the intercept x_0 shows multiple solutions, both for $x_0 > 0$ and $x_0 < 0$. This clearly illustrates the necessity for a Monte Carlo approach, which can sample multiple solutions over a much larger range of parameter space. For the KP off-shell function, the distribution for the normalization C is generally confined to negative values, while the solutions for x_0 are strongly peaked and appear to be somewhat anticorrelated with the values found for the CJ result.

From these fitted parameters, the resulting off-shell functions δf^p and δf^n are computed in Fig. 11, for both the CJ and KP off-shell isoscalar distributions δf^0. In the kinematic region constrained by the E03-103 data, $0.3 \lesssim x \lesssim 0.6$, the proton off-shell function δf^p is found to be positive and significantly larger than the isoscalar function δf^0 for both CJ and KP fits. Consequently, from Eq. (46) the neutron off-shell function δf^n becomes negative [see the second term in (46)], with its magnitude enhanced by the factor $F_2^p/F_2^n > 1$. For the CJ fit, the proton and neutron off-shell functions remain positive and negative, respectively, over the fitted range, while for the KP off-shell fit there is a sign change at $x \approx 0.4$.

Although the absolute values of the proton and neutron off-shell functions in Fig. 11 are large relative to the isoscalar functions, the respective contributions to the nucleon structure functions are weighted by the nucleon virtuality $v(p^2) \ll 1$. For ^{3}He, the average proton and neutron virtualities (for the KPSV spectral function) are found to be $\approx -7\%$ and $\approx -9\%$, respectively. At the lower end of the x range covered by the experiment, the relative correction to the nucleon structure functions are $\lesssim$10%, and rise to $\approx$30% for the neutron at the higher x values. Off-shell corrections that are very large ($\gtrsim$30–50%) are likely to invalidate the lowest order expansion in v assumed in Eq. (10), or may suggest issues with the systematic uncertainties assigned to the ^{3}He/d data [33].

Taking into account the overall normalization uncertainty of the ^{3}He/d ratio data, the Monte Carlo distribution of the fitted data normalization parameter, N_{dat}, is shown in Fig. 12, with values restricted to lie within the 1.84% quoted for the E03-103 experiment [33]. For the fit using the CJ isoscalar function, the distribution is relatively broad, with a peak at around 1% and an average of $N_{\mathrm{dat}} = 1.006 \pm 0.009$. This gives a very good overall fit to the E03-103 data, as evident from Fig. 9. For the KP off-shell function, the normalization parameter distribution is more concentrated at the upper limit, with an average $N_{\mathrm{dat}} = 1.012 \pm 0.005$. The resulting fit to the ^{3}He/d data is not quite as good at the lower x values, but still consistent with the data within 1σ.

Note that the full Monte Carlo fit clearly disfavors zero off-shell corrections, $C = 0$, especially for the CJ isoscalar function, since it is easier for the fit to vary one of the free parameters than to keep the same shape and compensate by a normalization shift in the data. Nevertheless, if the off-shell corrections are switched off "by hand," one can still obtain a good fit to the ^{3}He/d data with just the on-shell contributions, as illustrated in Fig. 9, with an average data normalization shift $N_{\mathrm{dat}} = 1.016 \pm 0.002$, consistent with the maximum 1.84% allowed [see Fig. 12]. The χ^2/dof value for the on-shell fit is slightly larger than that for the off-shell fit, but is still <1 and within 1σ from the best fit, even though the tendency is towards a shape with a slightly different slope than the data prefer.

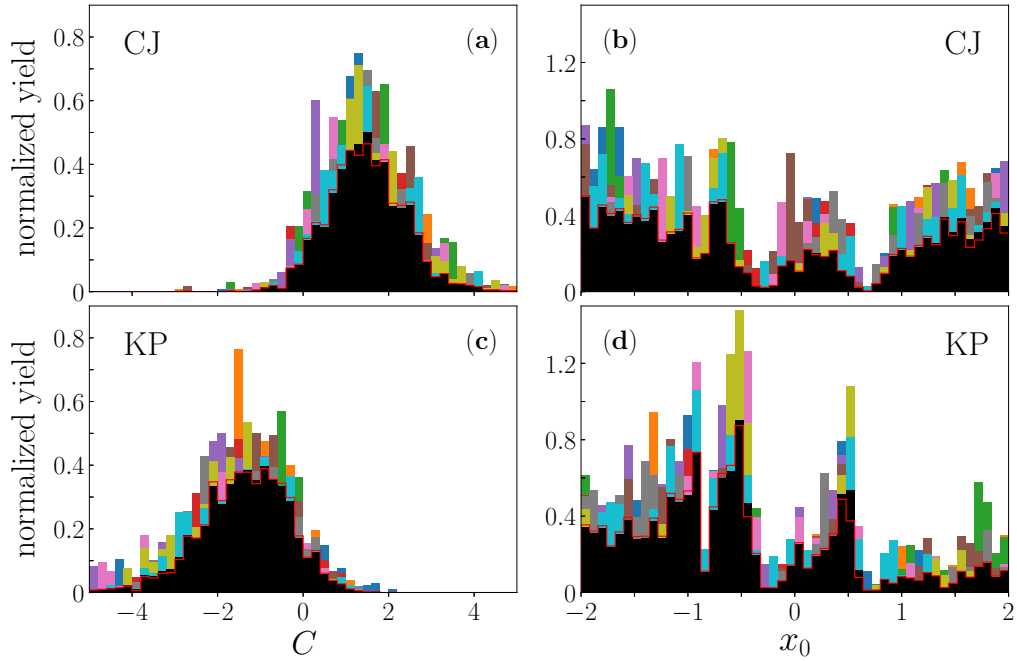

FIG. 10. Normalized yield of the Monte Carlo parameter distributions for the proton off-shell function δf^p, for the normalization C [(a) and (c)] and intercept x_0 [(b) and (d)], using the isoscalar off-shell function δf^0 from the CJ [15] [(a) and (b)] and KP [25] [(c) and (d)] analyses. The colored histograms represent 10 statistically independent Monte Carlo analyses, while the black histograms are the combined result.

In an earlier analysis of the E03-103 ^{3}He/d ratio, Kulagin and Petti showed [34] that with the KP off-shell correction, and assuming $\delta f^p = \delta f^n$, one could fit the Seely *et al.* data with a 3% normalization shift, and be consistent with extractions of F_2^n/F_2^p from NMC data. This value lies outside of the 1σ range for $N_{\rm dat}$ quoted by the experiment. Using our Monte Carlo methodology, we also attempt to fit the E03-103 data using the isospin symmetric KP off-shell function. Constraining the normalization $N_{\rm dat}$ to be within the quoted experimental uncertainty range, the fit shown in Fig. 12 prefers the maximum upward shift of the data, with an average value $N_{\rm dat} = 1.016 \pm 0.001$. The resulting $\sigma^{^3{\rm He}}/\sigma^d$ ratio does not give as good a description of the data in Fig. 9, overestimating the ratio at lower x and underestimating it at higher x. If one uses instead the CJ isoscalar off-shell correction, assuming isospin symmetry, the fitted data normalization is also near the maximum allowed, $N_{\rm dat} = 1.017 \pm 0.001$. The resulting fit to the ^{3}He/d data in Fig. 9 shows good agreement at lower x but overestimates the data at the higher x values.

The inescapable conclusion is that, taking the E03-103 ^{3}He/d data [33] with the quoted uncertainties at face value, the fits clearly disfavor isospin symmetric off-shell corrections and slightly favor isospin -dependent off-shell effects over no off-shell corrections. In the next section, we examine the consequences of this for the MARATHON experiment and the extraction of the neutron to proton structure function ratio.

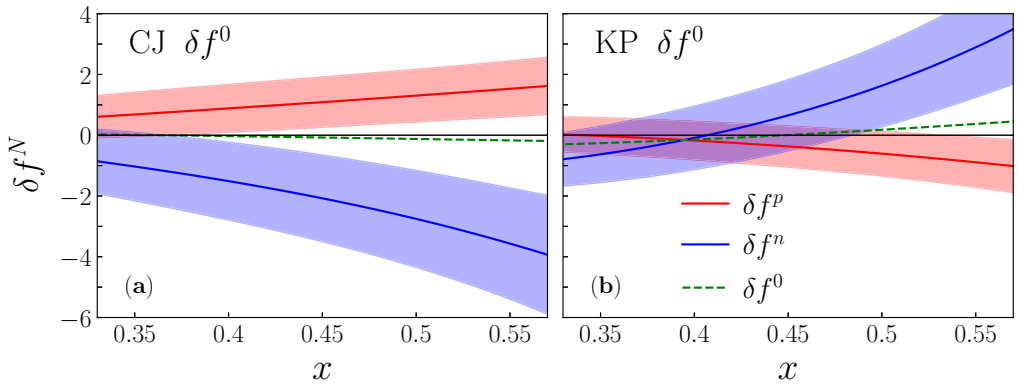

FIG. 11. Off-shell functions for the proton, δf^p (red solid curves and bands), and neutron, δf^n (blue solid curves and bands), from the fit to the E03-103 data [33], for a given isoscalar off-shell function, δf^0 (green dashed), from (a) the CJ [15] global analysis and (b) the Kulagin-Petti [25] nuclear ratios fit. The functions are shown only in the range of x constrained by the E03-103 data.

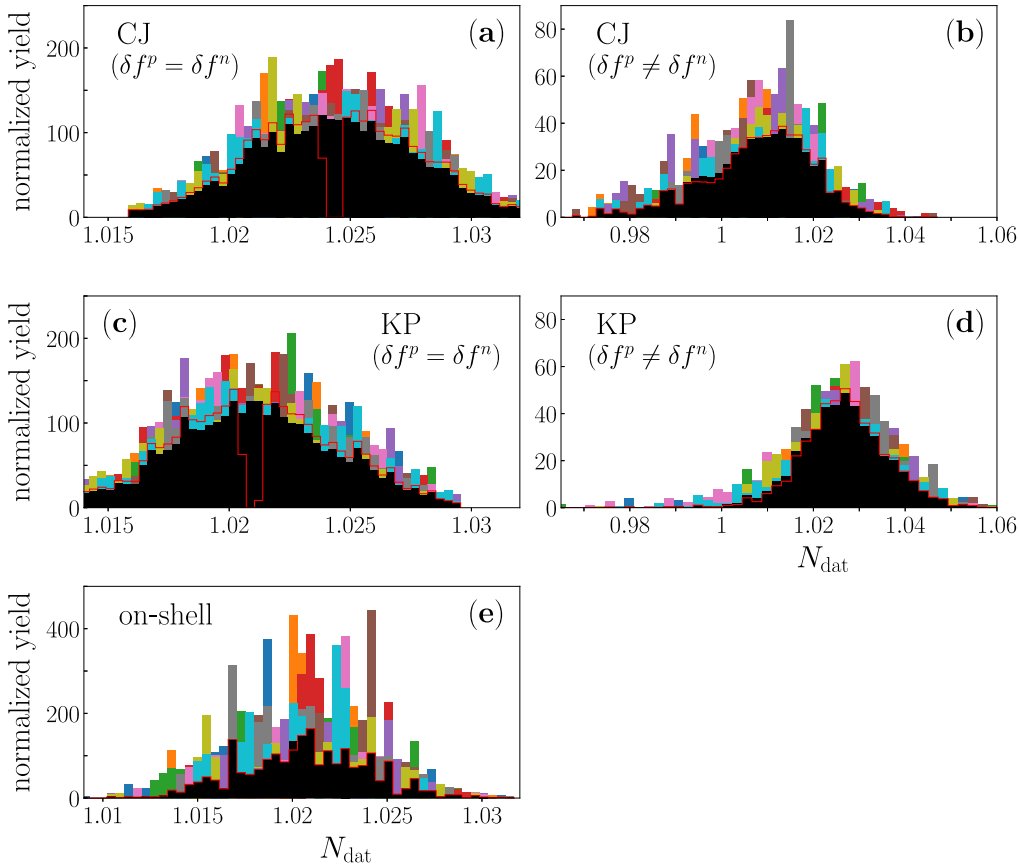

FIG. 12. Normalized yield of Monte Carlo distributions for the data normalization factors $N_{\rm dat}$ for the CJ [15] [(a) and (b)] and KP [25] [(c) and (d)] isoscalar functions δf^0, assuming isospin symmetry ($\delta f^p = \delta f^n$) [(a) and (c)] and the isospin-dependent analysis ($\delta f^p \neq \delta f^n$) [(b) and (d)], along with the on-shell only fit [(e)]. The colored histograms represent 10 statistically independent Monte Carlo analyses, while the black histograms are for the combined result. The pile-up in some of the fits occurs at the upper boundary of the allowed 1.84% normalization uncertainty in the E03-103 experiment [33].

C. Implications for $A = 3$ structure functions

Having obtained the constraints on the nucleon off-shell functions from the E01-103 ^{3}He/d data [33] and the previously determined isoscalar off-shell function, we next discuss the implications of these results for the structure functions of $A = 3$ nuclei. In particular, the MARATHON experiment [20] at Jefferson Lab will make high-precision measurements of the inclusive cross-section ratios for ^{3}He to ^{3}H, as well as ^{3}He/d and ^{3}H/d, which are expected to yield information on the ratio of the free neutron to proton structure functions. If one uses the super-ratio method in Eq. (39), the effect of the off-shell corrections extracted in Sec. IV B on the $\mathcal{R}$ ratio will therefore be of direct relevance for the n/p determination.

For the on-shell only calculation, Fig. 13 shows rather similar ^{3}He and ^{3}H EMC ratios, with both $R(^3\text{He})$ and $R(^3\text{H})$ having minima at $x \approx 0.5$–0.6, at which they dip $\approx$ 4–5% below unity, before rising rapidly at $x \gtrsim 0.7$ through Fermi motion. Because of the greater sensitivity of the ^{3}He and ^{3}H ratios to any isospin dependence of off-shell effects, including the off-shell corrections from Fig. 11 gives rise to some quite interesting features. Since the ^{3}He ratio is more sensitive to proton structure than to the neutron, for the case of the CJ isoscalar off-shell correction the fitted positive proton off-shell function δf^p induces a slightly stronger EMC effect, with the dip in $R(^3\text{He})$ increasing to $\approx$5%. In contrast, since the neutron plays a greater role in the ^{3}H EMC ratio, the fitted negative neutron off-shell correction δf^n reduces the dip in $R(^3\text{H})$ to $\lesssim$2% for $x \lesssim 0.5$, with an earlier onset of the Fermi motion rise above unity.

For the KP isoscalar off-shell function δf^0, which gives similarly small fitted proton and neutron off-shell corrections at $0.3 \lesssim x \lesssim 0.4$, but increasing magnitudes for the (positive) neutron δf^n and (negative) proton δf^p at larger x, the effect on the ^{3}He and ^{3}H EMC ratios is more dramatic. In particular, the positive neutron off-shell function enhances the magnitude of the dip in the $R(^3\text{H})$ ratio to almost 10% at $x \approx 0.65$, in marked contrast to the prediction with the CJ δf^0. The impact on the $R(^3\text{He})$ ratio is much less at large x, with little deviation of the KP off-shell result from the on-shell fit at $x \gtrsim 0.4$. At smaller x values, $x \lesssim 0.3$, the KP off-shell corrections yield an enhancement of $\approx$2–3% above unity in both the ^{3}He and ^{3}H ratios, which is directly related to the dip in the KP δf^0 function at $x \approx 0.2$ seen in Fig. 8. On the other hand, there is currently no compelling evidence for such an enhancement from deuterium data [15], and the effect in the KP δf^0 may be due to the use of data on heavy nuclei in

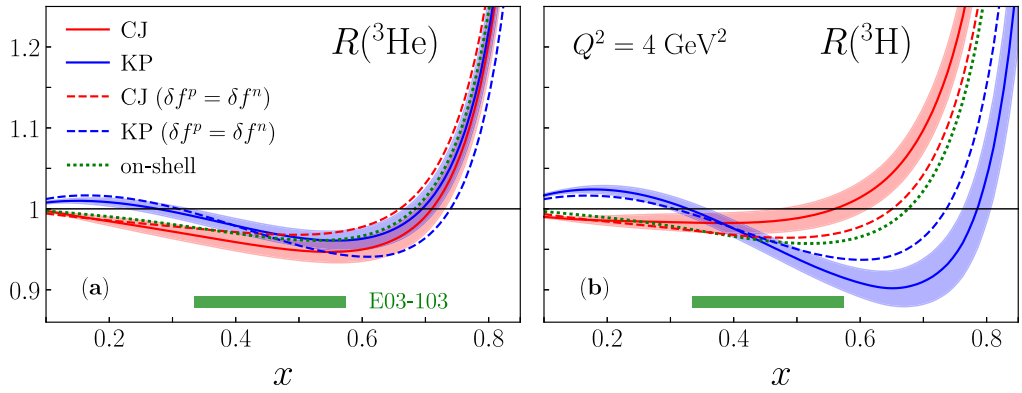

FIG. 13. Ratios of nuclear to nucleon structure functions (a) $R(^3\mathrm{He}) = F_2^{^3\mathrm{He}}/(2F_2^p + F_2^n)$ and (b) $R(^3\mathrm{H}) = F_2^{^3\mathrm{H}}/(F_2^p + 2F_2^n)$, for the off-shell Monte Carlo fits using the CJ [15] (solid red curves and bands) and Kulagin-Petti [25] (solid blue curves and bands) isoscalar off-shell function δf^0, compared with the ratios assuming isospin symmetric off-shell functions from CJ (dashed red curves) and KP (dashed blue curves), and the on-shell only fit (dotted green curves). The range of x constrained by the Jefferson Lab E03-103 experiment [33] is indicated by the green horizontal band, and a scale of $Q^2 = 4$ GeV^2, which is close to the average for the E03-103 data, was used for all structure functions.

the KP analysis [25], which do display some enhancement of F_2^A/F_2^d at $x \sim 0.1$–0.2.

Note also that the off-shell corrections are constrained by the E03-103 data [33] only in the range between $x \approx 0.3$ and 0.6, and outside this range, where the low-x enhancement for the KP case and the growing differences between the $R(^3\mathrm{H})$ ratios at large x are apparent, these are not directly constrained by data. Measurement of the ^{3}H structure function in the MARATHON experiment [20], covering a wide range of x values, $0.2 \lesssim x \lesssim 0.8$, will provide an unprecedented opportunity to examine the role of nucleon off-shell effects in the $A = 3$ system, as well as their possible isospin dependence. In fact, as Fig. 13 illustrates, the $R(^3\mathrm{He})$ and $R(^3\mathrm{H})$ ratios show sensitivity to the off-shell corrections even if these are assumed to be isospin symmetric, $\delta f^0 = \delta f^p = \delta f^n$. In the case of δf^0 determined from the CJ analysis [15], the off-shell corrections move both the ^{3}He and ^{3}H ratios upward relative to the on-shell calculation, resulting in slightly weaker EMC effects for both nuclei. For δf^0 taken from the KP analysis [25], the effect is a downward shift, making the EMC effects in ^{3}He and ^{3}H slightly larger. Consequently, the relative shifts in $R(^3\mathrm{He})$ and $R(^3\mathrm{H})$ in both models are similar.

This can be more directly seen in the super-ratio, $\mathcal{R} = R(^3\mathrm{He})/R(^3\mathrm{H})$, of the ^{3}He and ^{3}H EMC ratios, in Fig. 14. For both the on-shell only and isospin symmetric off-shell fits, the super-ratio is within $\approx$1% of unity for $x \lesssim 0.7$, with the deviations increasing slightly at larger x values. (Recall, however, from Fig. 9 that the fits to the E03-103 data [33] with the isospin symmetric off-shell corrections give the worst agreement, especially for the KP isoscalar correction.) For the isospin asymmetric off-shell functions, the deviations from unity are at the few-percent level up to $x \approx 0.4$, but become significantly larger at higher x, reaching $\approx$15% above unity at $x = 0.8$ for the CJ fit, and a similar amount below unity for the KP result, albeit with large uncertainties. This translates to a ratio of ^{3}He to ^{3}H structure functions, which will be extracted

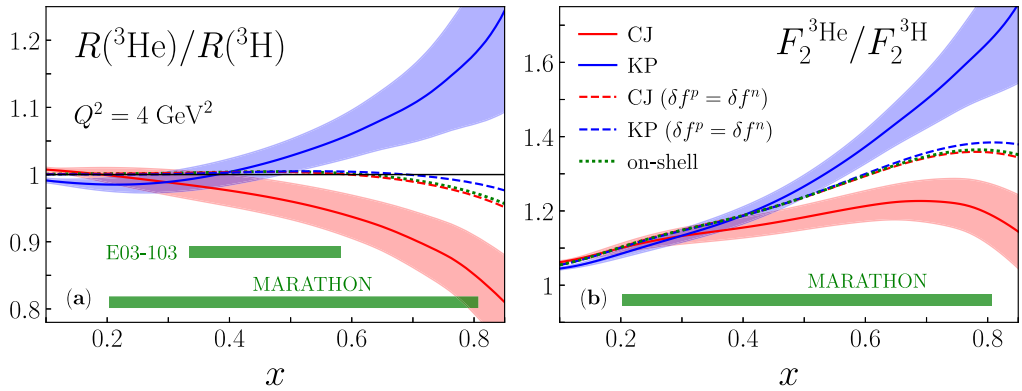

FIG. 14. (a) Super-ratio $R(^3\mathrm{He})/R(^3\mathrm{H})$ of the EMC ratios in ^{3}He and ^{3}H and (b) the ratio $F_2^{^3\mathrm{He}}/F_2^{^3\mathrm{H}}$ of the ^{3}He and ^{3}H structure functions. The off-shell Monte Carlo fits using the CJ [15] (solid red curves and bands) and Kulagin-Petti [25] (solid blue curves and bands) isoscalar off-shell functions δf^0 are compared with the results assuming isospin symmetric off-shell functions from CJ (dashed red curves) and KP (dashed blue curves), and the on-shell only fit (dotted green curves). The range of x constrained by the Jefferson Lab E03-103 experiment [33] and the extended range expected by the MARATHON experiment [20] are indicated by the green horizontal bands.

from the MARATHON experiment, that deviates from the on-shell result by up to $\approx -10\%$ for the CJ result and $\approx +20\%$ for the KP fit at $x = 0.8$, with $\approx 50\%$ statistical uncertainties on these values.

Of course, as discussed above, the results on the off-shell corrections are constrained by the E03-103 data only for $x \lesssim 0.6$, above which their extrapolation cannot be considered very reliable. In the region specifically covered by the E03-103 experiment [33], the off-shell effects scale up to $\approx 5\%$, although in opposite directions for the CJ and KP isoscalar off-shell corrections. Measurement of the ^{3}He/^{3}H ratio in MARATHON would therefore be vital for discriminating between these scenarios.

On the other hand, without additional assumptions it may be difficult to attribute the differences such as those in Fig. 14 entirely to different proton and neutron off-shell corrections, or to a different behavior of the free neutron structure function at large x. In the following, we discuss an alternative analysis scenario, in which the MARATHON data on the nuclear structure function ratios can be used as critical input for a simultaneous determination of both the neutron to proton ratio *and* the isospin dependence of the nucleon off-shell corrections.

D. Extracting neutron structure from MARATHON

While our Monte Carlo analysis suggests that the possibility of strong isospin dependence of the nucleon off-shell effects at high x cannot be ruled out on the basis of the E03-103 data [33], it is necessary to examine the caveats and assumptions that underlie these findings. First, our extraction of the proton and neutron off-shell functions δf^p and δf^n assumes the isoscalar nucleon off-shell correction δf^0 to be reliably determined from previous analyses of the proton and deuteron data (or, in the case of KP, also of heavy nuclear structure function ratios). However, as is obvious from the sizeable differences between the CJ and KP δf^0 functions in Fig. 8 and in their consequences for the super-ratio in Fig. 14, the magnitude of the isoscalar off-shell correction, and even its sign as a function of x, is controversial. Futhermore, in our analysis we have used the same set of input nucleon PDFs [15] with both the CJ and KP isoscalar off-shell functions. While this is consistent for the CJ δf^0, for the analysis with the KP off-shell function one should in principle use the PDF set that was used in the extraction of δf^0 in Ref. [25]. The KP analysis [25] assumed, however, that $\delta f^p = \delta f^n$ in the fits to structure function ratios for asymmetric nuclei, so using the KP δf^0 to determine the isospin dependence of δf^N in our analysis is not entirely consistent.

A more reliable determination of the proton and neutron off-shell corrections would involve a *simultaneous* analysis of proton, deuteron, and $A = 3$ nuclear data. This would remove many systematic effects arising from different theoretical assumptions and inputs utilized in the different analyses. Whatever tensions then remain between data sets in the combined fit would be treated consistently within the same analysis. In principle, while a global QCD analysis is the most natural framework in which to perform the simultaneous fit to the nucleon PDFs and nuclear off-shell functions, one could also imagine a more restricted fit at the structure function level.

In particular, with sufficient experimental information on the structure functions of ^{3}He, ^{3}H, and deuterium, one can in practice disentangle the nuclear effects from the on-shell nucleon structure functions. Within the convolution framework of Sec. II B, the nuclear structure functions are expressed as sums of on-shell and off-shell contributions, as in Eq. (17),

$$F_2^A(x, Q^2) = F_2^{A\,(\mathrm{on})}(x, Q^2) + F_2^{A\,(\mathrm{off})}(x, Q^2), \tag{47}$$

for $A = d$, ^{3}He, and ^{3}H. The on-shell term depends on the free proton and neutron structure functions, F_2^p and F_2^n, and the nuclear smearing functions, $f_{ij}^{N/A}$, in Eq. (13). The latter are reasonably well determined away from the tails of the distributions at large y, which become important only at $x \sim 1$. The off-shell term depends on F_2^p, F_2^n, δf^p, δf^n, and the off-shell smearing functions $\widetilde{f}_{ij}^{N/A}$ in Eq. (16), which are computed in terms of the *same* set of nuclear wave functions as the on-shell smearing functions $f_{ij}^{N/A}$.

Since the proton F_2^p structure function is well known, the three unknowns—the F_2^n/F_2^p ratio and the two off-shell corrections, δf^p and δf^n—can then be determined from three independent observables, such as the ratios ^{3}He/d and ^{3}H/d (or ^{3}He/^{3}H) and F_2^d/F_2^p. The ratios involving ^{3}He and ^{3}H are the main focus of the MARATHON experiment; however, the experiment will also measure the deuteron/proton structure function ratio over a more restricted range of kinematics, from $x = 0.18$ to 0.38 (for Q^2 between 2.5 and 5.3 GeV^2), which will be used to benchmark against the large body of high-precision data on inclusive F_2^d and F_2^p structure functions that has been accumulated over the past few decades [86].

While in global QCD analyses one typically parametrizes individual PDFs from which all observables are then constructed, for an analysis at the structure function level the x and Q^2 dependence of the structure functions could be parametrized by a form such as [87]

$$F_2(x, Q^2) = a_0(Q^2) x^{a_1(Q^2)} (1-x)^{a_2(Q^2)} (1 + a_3(Q^2)\sqrt{x} + a_4(Q^2)\, x + \cdots), \tag{48}$$

with Q^2-dependent shape parameters

$$a_i(Q^2) = a_i^{(0)} + a_i^{(1)} s(Q^2), \quad s(Q^2) = \log\left(\frac{\log(Q^2/\Lambda_{\mathrm{QCD}}^2)}{\log(\mu^2/\Lambda_{\mathrm{QCD}}^2)}\right), \tag{49}$$

for $i = 1$–4, where Λ_{QCD} is the QCD scale parameter, and μ^2 is a scale of order $\mathcal{O}(1\,\mathrm{GeV}^2)$ fitted to the data. For the proton and neutron off-shell functions a polynomial of degree 3, as in Eq. (44), would be expected to be sufficient. (For simplicity, one can assume that δf^N is independent of Q^2, so that the scale dependence of the off-shell contributions to the structure functions is the same as the on-shell.) The extraction of the three unknown functions would then involve fitting ≈ 30 parameters, which can be constrained within a Bayesian likelihood analysis. In this approach, recently employed by the JAM Collaboration in their Monte Carlo analyses of PDFs and fragmentation functions [80–84], the multivariate

probability density for a set of fit parameters $\boldsymbol{a} = \{a_i\}$ conditioned by the data is given by $p(\boldsymbol{a}|\text{data}) \propto \mathcal{L}(\text{data}|\boldsymbol{a})\,\pi(\boldsymbol{a})$, where the likelihood $\mathcal{L}$ is a Gaussian function of the χ^2,

$$\mathcal{L}(\text{data}|\boldsymbol{a}) = \exp\left[-\tfrac{1}{2}\chi^2(\boldsymbol{a}, \text{data})\right], \tag{50}$$

and $\pi(\boldsymbol{a})$ is the distribution of priors. The χ^2 function takes into account experimental statistical, systematic (uncorrelated and correlated), and normalization uncertainties for each data set used in the fit [80]. The expectation values and 1σ uncertainties for the fitted quantities can then be computed by Monte Carlo sampling of the probability density [83].

The remaining approximations in such an analysis are ones that reflect the validity of the convolution framework itself, as outlined in Sec. II B. Namely, one assumes that within the WBA the form of the off-shell nucleon function δf^N remains the same for both $A = 2$ and $A = 3$ nuclei, with the A dependence of the off-shell structure functions in Eqs. (15) entering only through the off-shell smearing function $\widetilde{f}_{ij}^{N/A}$. The model dependence of the smearing functions can be assessed by considering different wave functions or spectral functions for the deuteron and $A = 3$ nuclei, as we have explored for the KPSV and SS ^{3}He spectral functions in Sec. II C. Since the choice of wave function model is a discrete rather than a continuous parameter, it is difficult to systematically incorporate the uncertainty from this into the final error analysis. The usual procedure is to examine the dependence of the results on the choice of wave function and estimate the uncertainty from the resulting variation.

V. CONCLUSION

With the completion of data taking in 2018 by the suite of ^{3}He/^{3}H experiments at Jefferson Lab, including MARATHON in DIS kinematics [20] and E12-11-112 in the QE region and beyond, there is great anticipation to see the impact that the new data will have on our knowledge of the structure of the free neutron, and in particular on the d/u PDF ratio at large x, which has eluded definitive confirmation for more than three decades. Working within the weak binding approximation formalism, we have revisited the calculation of deep-inelastic $A = 3$ structure functions using the latest theoretical developments, in terms of finite-Q^2 convolution formulas and nuclear effects computed from $A = 3$ spectral functions and off-shell nucleon structure functions.

To test the veracity of the WBA smearing functions and the range of applicability of the impulse approximation, we have examined the world's available data on inclusive ^{3}He structure functions in the vicinity of $x \approx 1$, which is expected to be dominated by QE scattering. Comparison with existing data from SLAC and Jefferson Lab suggests that a good description can be obtained using the Q^2-dependent smearing functions as for DIS, for $Q^2 \gtrsim 1$ GeV^2 out to $x \approx 1.3$. For smaller Q^2, rescattering and meson exchange current effects are expected to be more important, while for $x \gg 1$ the effects of the off-shell corrections and other multinucleon correlations will play a greater role. This analysis provides confidence in the application of the nuclear model to the description of the $A = 3$ DIS and QE data and suggests that the extraction of neutron information from the MARATHON and E12-11-112 Jefferson Lab data should not be impeded by the lack of knowledge of the short-range structure of the $A = 3$ wave functions.

For the bound nucleon structure functions, the WBA formalism allows the inclusion of possible off-shell dependence in the calculation of the nuclear structure functions, in both DIS and QE kinematics. For the QE data comparisons, the off-shell corrections generally improve the agreement between data and the WBA theory, especially at low Q^2 values, irrespective of the prescription adopted for the elastic off-shell nucleon structure function. For the DIS region, the shape of the off-shell corrections for the isoscalar channel, δf^0, is taken from the earlier CJ15 global QCD analysis of proton and deuterium data [15] or from the Kulagin-Petti fit to various nuclear structure function ratios [25], which assumed isospin symmetry for the off-shell functions.

To explore possible constraints on the isospin dependence of the off-shell functions, we performed a Monte Carlo analysis of the recent data on the ^{3}He/d cross section ratios from the Jefferson Lab E03-103 experiment [33] for $0.33 \lesssim x \lesssim 0.58$. Within the statistical and systematic uncertainties of the data, one can obtain almost equally good descriptions with no off-shell corrections and with nonzero off-shell corrections with large cancellations between the proton and neutron contributions at large x. The analysis disfavors, however, fits with nonzero off-shell corrections which assume $\delta f^p = \delta f^n$. Unfortunately, the results are quite sensitive to the shape of the input isoscalar off-shell correction, and a robust analysis must therefore involve a simultaneous fit to all proton, deuteron and $A = 3$ data. Also, the lack of scatter of the E03-103 data points in Fig. 9 suggests that the data do not follow a Gaussian probability distribution, so that the uncertainties on the data points are dominated by systematic errors. This highlights the important need for the new high-precision data expected from the MARATHON experiment.

We have also outlined an analysis procedure for extracting the neutron structure function F_2^n using Bayesian methods that would be capable of simultaneously extracting the free neutron to proton structure function ratio and the proton and neutron off-shell functions, δf^p and δf^n, within the nuclear WBA framework. This would remove potential uncertainties in the extracted F_2^n propagating from any assumptions made about the super-ratio, $\mathcal{R}$, of the ^{3}He to ^{3}H EMC ratios. Instead, the method would utilize MARATHON data on the ^{3}He/d and ^{3}H/d ratios, as well as d/p measurements to be used for benchmarking against the global inclusive proton and deuteron DIS data sets. The MARATHON ratio data can also be supplemented with measurements of the absolute values of the F_2^p and F_2^d structure functions at similar kinematics in the E12-10-002 experiment [88] in Jefferson Lab's Hall C, for $x \gtrsim 0.2$ and $Q^2 \approx 5$–16 GeV^2. The new data are eagerly awaited and promise to reveal for the first time the detailed structure of the free neutron at large x, as well as the isospin dependence of the nuclear effects, and solve the long-standing problem of the size of the nuclear EMC effect in the deuteron.

ACKNOWLEDGMENTS

We thank D. Gaskell, C. Keppel, S. Li, H. Liu, G. Petratos and G. Schnel for helpful discussions and communications.

This work was supported by the US Department of Energy Contract No. DE-AC05-06OR23177, under which Jefferson Science Associates, LLC, operates Jefferson Lab. A.T. was supported by NSF Grant No. 1359026 for an REU internship at ODU/Jefferson Lab, University Fellowship from the Ohio State Graduate School, and the William A. Fowler Graduate Fellowship from the Ohio State Department of Physics. N.S. was supported by DOE Contract No. DE-FG-04ER41309. J.E. has been partly supported by the Netherlands Organization for Scientific Research (NWO).

[1] R. J. Holt and C. D. Roberts, Rev. Mod. Phys. **82**, 2991 (2010).
[2] M. E. Christy and W. Melnitchouk, J. Phys.: Conf. Ser. **299**, 012004 (2011).
[3] P. Jimenez-Delgado, W. Melnitchouk, and J. F. Owens, J. Phys. G: Nucl. Part. Phys. **40**, 093102 (2013).
[4] J. Gao, L. Harland-Lang, and J. Rojo, Phys. Rep. **742**, 1 (2018).
[5] W. Melnitchouk and A. W. Thomas, Phys. Lett. B **377**, 11 (1996).
[6] A. Accardi, W. Melnitchouk, J. F. Owens, M. E. Christy, C. E. Keppel, L. Zhu, and J. G. Morfin, Phys. Rev. D **84**, 014008 (2011).
[7] J. F. Owens, A. Accardi, and W. Melnitchouk, Phys. Rev. D **87**, 094012 (2013).
[8] J. Arrington, J. G. Rubin, and W. Melnitchouk, Phys. Rev. Lett. **108**, 252001 (2012).
[9] N. Baillie *et al.*, Phys. Rev. Lett. **108**, 199902 (2012).
[10] S. Tkachenko *et al.*, Phys. Rev. C **89**, 045206 (2014).
[11] D. Acosta *et al.*, Phys. Rev. D **71**, 051104(R) (2005).
[12] T. Aaltonen *et al.*, Phys. Rev. Lett. **102**, 181801 (2009).
[13] V. M. Abazov *et al.*, Phys. Rev. D **77**, 011106(R) (2008).
[14] V. M. Abazov *et al.*, Phys. Rev. Lett. **101**, 211801 (2008).
[15] A. Accardi, L. T. Brady, W. Melnitchouk, J. F. Owens, and N. Sato, Phys. Rev. D **93**, 114017 (2016).
[16] S. I. Alekhin, S. A. Kulagin, and R. Petti, Phys. Rev. D **96**, 054005 (2017).
[17] Jefferson Lab Experiment E12-10-102 [BONuS], S. Bültmann, M. E. Christy, H. Fenker, K. Griffioen, C. E. Keppel, S. Kuhn, and W. Melnitchouk, spokespersons.
[18] Jefferson Lab Experiment E12-10-007 [SoLID], P. Souder, spokesperson.
[19] T. J. Hobbs and W. Melnitchouk, Phys. Rev. D **77**, 114023 (2008).
[20] Jefferson Lab Experiment E12-10-103 [MARATHON], G. G. Petratos, J. Arrington, M. Katramatou, and R. D. Ransome, spokespersons.
[21] I. R. Afnan, F. R. P. Bissey, J. Gomez, A. T. Katramatou, W. Melnitchouk, G. G. Petratos, and A. W. Thomas, Phys. Lett. B **493**, 36 (2000).
[22] I. R. Afnan, F. R. P. Bissey, J. Gomez, A. T. Katramatou, S. Liuti, W. Melnitchouk, G. G. Petratos, and A. W. Thomas, Phys. Rev. C **68**, 035201 (2003).
[23] E. Pace, G. Salme, S. Scopetta, and A. Kievsky, Phys. Rev. C **64**, 055203 (2001).
[24] M. M. Sargsian, S. Simula, and M. I. Strikman, Phys. Rev. C **66**, 024001 (2002).
[25] S. A. Kulagin and R. Petti, Nucl. Phys. A **765**, 126 (2006).
[26] S. A. Kulagin and W. Melnitchouk, Phys. Rev. C **78**, 065203 (2008).
[27] J. J. Ethier and W. Melnitchouk, Phys. Rev. C **88**, 054001 (2013).
[28] H. J. Pirner and J. P. Vary, Phys. Rev. Lett. **46**, 1376 (1981).
[29] T. de Forest and P. J. Mulders, Phys. Rev. D **35**, 2849 (1987).
[30] M. Sato, S. A. Coon, H. J. Pirner, and J. P. Vary, Phys. Rev. C **33**, 1062 (1986).
[31] K. Maltman, G. J. Stephenson, and J. T. Goldman, Phys. Lett. B **324**, 1 (1994).
[32] C. J. Benesh, T. Goldman and G. J. Stephenson, Jr., Phys. Rev. C **68**, 045208 (2003).
[33] J. Seely *et al.*, Phys. Rev. Lett. **103**, 202301 (2009).
[34] S. A. Kulagin and R. Petti, Phys. Rev. C **82**, 054614 (2010).
[35] D. Day, J. S. McCarthy, I. Sick, R. G. Arnold, B. T. Chertok, S. Rock, Z. M. Szalata, F. Martin, B. A. Mecking, and G. Tamas, Phys. Rev. Lett. **43**, 1143 (1979).
[36] Z. E. Meziani, J. P. Chen, D. Beck, G. Boyd, L. M. Chinitz, D. B. Day, L. C. Dennis, G. E. Dodge, B. W. Fillipone, K. L. Giovanetti *et al.*, Phys. Rev. Lett. **69**, 41 (1992).
[37] N. Fomin *et al.*, Phys. Rev. Lett. **105**, 212502 (2010).
[38] Jefferson Lab Experiment E12-11-112, D. Higinbotham, J. Arrington, D. Day and Z. Ye, spokespersons.
[39] S. A. Kulagin, G. Piller, and W. Weise, Phys. Rev. C **50**, 1154 (1994).
[40] S. A. Kulagin, W. Melnitchouk, G. Piller, and W. Weise, Phys. Rev. C **52**, 932 (1995).
[41] S. A. Kulagin and W. Melnitchouk, Phys. Rev. C **77**, 015210 (2008).
[42] W. Melnitchouk, A. W. Schreiber, and A. W. Thomas, Phys. Rev. D **49**, 1183 (1994).
[43] W. Melnitchouk, A. W. Schreiber, and A. W. Thomas, Phys. Lett. B **335**, 11 (1994).
[44] O. Nachtmann, Nucl. Phys. B **63**, 237 (1973).
[45] O. W. Greenberg and D. Bhaumik, Phys. Rev. D **4**, 2048 (1971).
[46] R. P. Bickerstaff and A. W. Thomas, J. Phys. G **15**, 1523 (1989).
[47] P. J. Ehlers, A. Accardi, L. T. Brady, and W. Melnitchouk, Phys. Rev. D **90**, 014010 (2014).
[48] F. R. P. Bissey, A. W. Thomas, and I. R. Afnan, Phys. Rev. C **64**, 024004 (2001).
[49] J. Haidenbauer and W. Plessas, Phys. Rev. C **30**, 1822 (1984).
[50] T. Y. Saito and I. R. Afnan, Few-Body Syst. **18**, 101 (1995).
[51] R. V. Reid, Ann. Phys. (NY) **50**, 411 (1968).
[52] Y. Yamaguchi and Y. Yamaguchi, Phys. Rev. **95**, 1635 (1954).
[53] R.-W. Schulze and P. U. Sauer, Phys. Rev. C **48**, 38 (1993).
[54] A. Stadler, W. Glöckle, and P. U. Sauer, Phys. Rev. C **44**, 2319 (1991).
[55] C. Ciofi degli Atti, E. Pace, and G. Salme, Phys. Rev. C **21**, 805 (1980).
[56] C. Ciofi degli Atti, E. Pace, and G. Salme, Phys. Lett. B **141**, 14 (1984).
[57] A. Kievsky, E. Pace, G. Salmè, and M. Viviani, Phys. Rev. C **56**, 64 (1997).
[58] A. Kievsky, M. Viviani, and S. Rosati, Nucl. Phys. A **551**, 241 (1993).
[59] T. De Forest, Nucl. Phys. A **392**, 232 (1983).
[60] O. Benhar, D. Day, and I. Sick, arXiv:nucl-ex/0603032; http://faculty.virginia.edu/qes-archive
[61] K. Dow, S. Dytman, D. Beck, A. Bernstein, I. Blomqvist, H. Caplan, D. Day, M. Deady, P. Demos, W. Dodge *et al.*, Phys. Rev. Lett. **61**, 1706 (1988).
[62] C. Marchand *et al.*, Phys. Lett. B **153**, 29 (1985).

[63] J. J. Kelly, Phys. Rev. C **70**, 068202 (2004).
[64] J. J. Ethier, N. Doshi, S. Malace, and W. Melnitchouk, Phys. Rev. C **89**, 065203 (2014).
[65] J. Arrington, W. Melnitchouk, and J. A. Tjon, Phys. Rev. C **76**, 035205 (2007).
[66] S. Venkat, J. Arrington, G. A. Miller, and X. Zhan, Phys. Rev. C **83**, 015203 (2011).
[67] P. E. Bosted, Phys. Rev. C **51**, 409 (1995).
[68] M. E. Christy and P. E. Bosted, Phys. Rev. C **81**, 055213 (2010).
[69] P. J. Mulders, A. W. Schreiber, and H. Meyer, Nucl. Phys. A **549**, 498 (1992).
[70] L. Frankfurt and M. Strikman, Phys. Rep. **160**, 235 (1988).
[71] F. E. Close, R. G. Roberts, and G. G. Ross, Phys. Lett. B **129**, 346 (1983).
[72] F. E. Close, R. L. Jaffe, R. G. Roberts, and G. G. Ross, Phys. Rev. D **31**, 1004 (1985).
[73] R. B. Wiringa, V. G. J. Stoks, and R. Schiavilla, Phys. Rev. C **51**, 38 (1995).
[74] R. Machleidt, Phys. Rev. C **63**, 024001 (2001).
[75] F. Gross and A. Stadler, Phys. Rev. C **78**, 014005 (2008); **82**, 034004 (2010).
[76] M. Lacombe, B. Loiseau, R. Vinh Mau, J. Cote, P. Pires, and R. de Tourreil, Phys. Lett. B **101**, 139 (1981).
[77] J. Skilling, Nested sampling for general Bayesian computation [http://www.inference.phy.cam.ac.uk/bayesys]
[78] P. Mukherjee, D. Parkinson, and A. R. Liddle, Astrophys. J. **638**, L51 (2006).
[79] R. Shaw, M. Bridges, and M. P. Hobson, Mon. Not. Roy. Astron. Soc. **378**, 1365 (2007).
[80] N. Sato, W. Melnitchouk, S. E. Kuhn, J. J. Ethier, and A. Accardi, Phys. Rev. D **93**, 074005 (2016).
[81] J. J. Ethier, N. Sato, and W. Melnitchouk, Phys. Rev. Lett. **119**, 132001 (2017).
[82] P. C. Barry, N. Sato, W. Melnitchouk, and C. R. Ji, Phys. Rev. Lett. **121**, 152001 (2018).
[83] N. Sato, J. J. Ethier, W. Melnitchouk, M. Hirai, S. Kumano, and A. Accardi, Phys. Rev. D **94**, 114004 (2016).
[84] H. W. Lin, W. Melnitchouk, A. Prokudin, N. Sato, and H. Shows, Phys. Rev. Lett. **120**, 152502 (2018).
[85] See data table at `https://hallcweb.jlab.org/experiments/E03103/lightnuclei_paper/`
[86] S. Li *et al.* (unpublished).
[87] D. W. Duke and J. F. Owens, Phys. Rev. D **30**, 49 (1984).
[88] Jefferson Lab Experiment E12-10-002, M. E. Christy, C. E. Keppel, S. Malace, and I. Niculescu, spokespersons.